Journal of Sound and Vibration 326 (2009) 647–670

Contents lists available at ScienceDirect

Journal of Sound and Vibration

journal homepage: www.elsevier.com/locate/jsvi

Vibration analysis of piecewise straight thin-walled box beams without using artificial joint springs

Gang-Won Jang [a], Yoon Young Kim [b,*]

[a] School of Mechanical and Automotive Engineering, Kunsan National University, Kunsan, Jeonbuk 573-701, Republic of Korea
[b] School of Mechanical and Aerospace Engineering and National Creative Research Initiatives Center for Multiscale Design, Seoul National University, San 56-1, Shillim-dong, Kwanak-gu, Seoul 151-742, Korea

ARTICLE INFO

Article history:
Received 21 January 2009
Received in revised form
27 April 2009
Accepted 2 May 2009
Handling Editor: L.G. Tham
Available online 3 June 2009

ABSTRACT

This investigation presents a vibration analysis of a thin-walled box beam system having angled joints by employing a higher-order beam theory that incorporates warping and distortional degrees of freedom (dof) in addition to the standard Timoshenko dof. In the proposed approach, no artificial spring is inserted between beams connected at an angled joint, but a systematic technique to match all dof of the connected beams is employed. There were similar efforts for static problems, but the vibration analysis using a higher-order beam theory without using joint springs is carried out here for the first time. Three cases were investigated: two box beams connected at an angled joint, a curved box beam modeled by several straight box beams each of which meets an adjacent beam at an angled joint, and a box beam forming a closed loop. The predicted vibration results by the developed approach were compared with shell analysis results.

1. Introduction

Fig. 1(a) illustrates two thin-walled box beams connected through an angled joint. Beam-based analysis for such a system has attracted the interest of many researchers for various reasons. For example, in a very initial stage of automobile body design, a simplified body-in-white (BIW) model consisting of beam and plate/shell elements is preferred (see, e.g., [1–4]). However, it is impossible to predict the vibration characteristics of a BIW accurately if a system of thin-walled closed pillars and rails is modeled only by conventional six-degree of freedom beams. Because conventional beam theories cannot account for cross-section deformations occurring especially near an angled joint, they predict too stiff structural beam behavior. Consequently, the predicted eigenfrequencies by the conventional theories tend to be considerably higher than the actual values and some eigenmodes are even missing. Therefore, the so-called joint springs, artificial elements, have been introduced between beams meeting at angled joints to account for joint effects. There are a number of investigations to estimate the spring stiffness [5–8], but it is impossible to correctly predict the flexibility effect of angled joints uniformly valid for a range of frequencies. In other words, one can estimate the spring stiffness that matches one or two eigenfrequencies, not all eigenfrequencies of interest.

The main objective of this investigation is to carry out the vibration analysis of piecewise straight thin-walled box beams connected at a finite number of angled joints only by a beam theory without using artificial joint springs. To this end, a higher-order beam theory having more dof than the Timoshenko beam theory is employed. A higher-order beam

* Corresponding author. Tel.: +82 2 880 7154; fax: +82 2 883 1513.
E-mail addresses: gangwon@kunsan.ac.kr (G.-W. Jang), yykim@snu.ac.kr (Y.Y. Kim).

0022-460X/$ - see front matter © 2009 Elsevier Ltd. All rights reserved.
doi:10.1016/j.jsv.2009.05.006

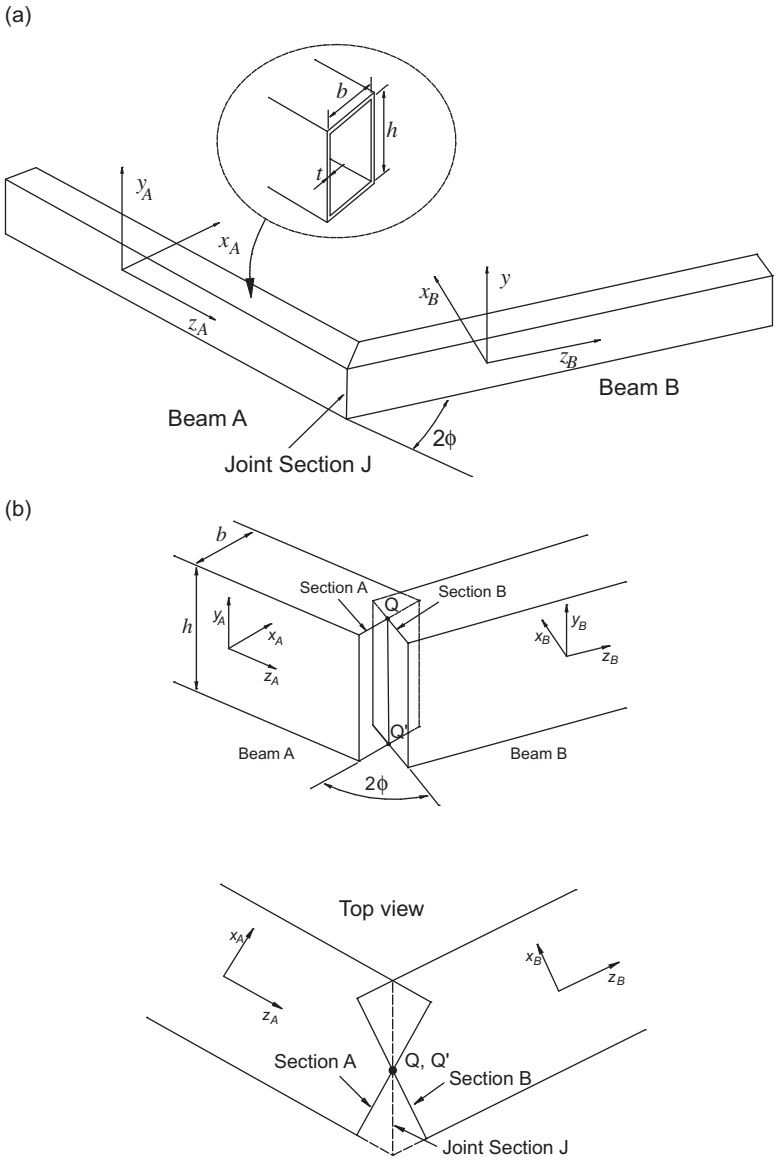

Fig. 1. (a) Thin-walled box beams connected at an angled joint and (b) a joint model consistent with a higher-order beam theory.

theory should include dof capable of representing cross-sectional deformations of warping and distortion. Earlier, the sectional shape functions corresponding to warping and distortional dof were derived for quadrilateral closed cross-sections [9] and for generally-shaped closed cross-sections [10]. The resulting one-dimensional vibration analysis taking the warping and distortional dof into account was shown to give favorable results for straight beams without a joint. The theory was also applied for the vibration analysis of a box beam T-joint [11]. The predicted eigenfrequencies by Kim et al. [11] were quite accurate, but this method still needed a special element contracted from a detailed shell model. Consequently, no existing paper seems to have conducted the vibration analysis of thin-walled closed beams without special joint elements.

If no special joint element is to be introduced, the dof of two adjacent beams meeting at an angled joint must be directly connected. In this case, the issue is how to impose the interface relation at the joint. The main difficulty appears when warping and distortional dof are to be matched; unlike bending or torsional dof having nonzero force resultants, warping and distortional dof have self-equilibrated force resultants. Therefore, the warping and distortional dof of two adjacent box beams cannot be matched simply by considering the vector calculus of their force resultants. Recently, Jang et al. [12] and Jang and Kim [13] have suggested joint interface relations for the warping and distortional dof by minimizing the difference

between the three-dimensional displacements of two adjacent beams at an imaginary common interface section of the angled joint. This section is denoted by Joint Section J in Fig. 1(b). However, no procedure for vibration analysis was presented in their works.

In this investigation, the sectional deformation shapes and interfacing conditions given by Jang et al. [12] and Jang and Kim [13] are employed to establish the vibration analysis of thin-walled closed box beams connected at an arbitrary angle. We will consider not only in-plane but also out-of-plane vibrations. When thin-walled box beams are connected in the same plane, the two types of vibrations are decoupled. Therefore, the kinetic energy and the strain energy of a beam system connected at a joint can be decomposed into in-plane and out-of-plane parts, respectively. Therefore, the mass and stiffness matrices of the beam system can be expressed separately for in-plane and out-of-plane deformations. This means that the interface relations at Joint Section J are also decoupled between in-plane and out-of-plane cases. Because the higher-order thin-walled beam elements are connected through the interface condition, there is no need to use artificial joints. The joint flexibility should be properly represented if the interface conditions are correct.

In Section 2, a higher-order beam theory for a straight thin-walled box beam under in-plane and out-of-plane bending deformations is presented along with its finite element formulation. In particular, the explicit forms of mass and stiffness matrices for linear higher-order beam elements are derived. Section 3 gives the interface relations at an angled joint between all field variables at Section A and those at Section B in Fig. 1(b) by setting up a minimization problem for the three-dimensional displacements on Joint Section J. To verify the validity of the developed joint element-less beam analysis for thin-walled box beams connected at angled joints, several numerical examples are considered. The predicted results by the developed approach are compared with those obtained by the Timoshenko beam elements as well as those by detailed shell elements. Concluding remarks are given in Section 5.

2. 10-DOF straight thin-walled beam theory and finite element implementation

In this section, the one-dimensional higher-order theory [12,13] for a rectangular thin-walled straight beam will be presented and a finite element implementation based on the theory will be developed. Figs. 2 and 3 illustrate the displacements of a box beam cross-section corresponding to 10 kinematic variables to be used for the higher-order beam analysis. Five variables describing in-plane deformations are U (extension), V^I (in-plane bending deflection), β^I (in-plane bending/shear rotation), W^I (in-plane bending warping), and χ^I (in-plane bending distortion). Five variables describing out-of-plane deformations are V^O (out-of-plane bending deflection), β^O (out-of-plane bending/shear rotation), θ (torsional rotation), W^O (torsional warping), and χ^O (torsional distortion). Among these 10 variables, U, V^I, β^I, V^O, β^O, and θ represent rigid-body displacements/rotations of a box beam cross-section while (W^I and W^O) and (χ^I and χ^O) represent non-rigid-body displacements of a cross-section. Note that out-of-plane bending warping and out-of-plane bending distortion are not considered because those deformations are higher energy modes. The sectional displacement patterns will be denoted by ψ's of which the explicit forms are given in Appendix A along with Eqs. (2) and (3).

Because in-plane and out-of-plane displacements can be decoupled in straight box beams, the three-dimensional displacements of the centerline of the cross-section can be written as the sum of the two parts:

$$u_n(s,z) = u_n^I(s,z) + u_n^O(s,z), \tag{1a}$$

$$u_s(s,z) = u_s^I(s,z) + u_s^O(s,z), \tag{1b}$$

$$u_z(s,z) = u_z^I(s,z) + u_z^O(s,z), \tag{1c}$$

where n and s denote the normal and tangential coordinates along the centerline of the cross-section, respectively, and z is the axial coordinate (see Fig. 4). In Eqs. (1), $u_\alpha^I(s,z)$ and $u_\alpha^O(s,z)$ ($\alpha = n,s,z$) refer to displacements in the direction of α induced by in-plane and out-of-plane deformations, respectively. They are given as

$$u_n^I(s,z) = \psi_n^U(s)U(z) + \psi_n^{VI}(s)V^I(z) + \psi_n^{\beta I}(s)\beta^I(z) + \psi_n^{WI}(s)W^I(z) + \psi_n^{\chi I}(s)\chi^I(z), \tag{2a}$$

$$u_s^I(s,z) = \psi_s^U(s)U(z) + \psi_s^{VI}(s)V^I(z) + \psi_s^{\beta I}(s)\beta^I(z) + \psi_s^{WI}(s)W^I(z) + \psi_s^{\chi I}(s)\chi^I(z), \tag{2b}$$

$$u_z^I(s,z) = \psi_z^U(s)U(z) + \psi_z^{VI}(s)V^I(z) + \psi_z^{\beta I}(s)\beta^I(z) + \psi_z^{WI}(s)W^I(z) + \psi_z^{\chi I}(s)\chi^I(z), \tag{2c}$$

and

$$u_n^O(s,z) = \psi_n^{Vo}(s)V^O(z) + \psi_n^{\beta o}(s)\beta^O(z) + \psi_n^{\theta}(s)\theta(z) + \psi_n^{Wo}(s)W^O(z) + \psi_n^{\chi o}(s)\chi^O(z), \tag{3a}$$

$$u_s^O(s,z) = \psi_s^{Vo}(s)V^O(z) + \psi_s^{\beta o}(s)\beta^O(z) + \psi_s^{\theta}(s)\theta(z) + \psi_s^{Wo}(s)W^O(z) + \psi_s^{\chi o}(s)\chi^O(z), \tag{3b}$$

$$u_z^O(s,z) = \psi_z^{Vo}(s)V^O(z) + \psi_z^{\beta o}(s)\beta^O(z) + \psi_z^{\theta}(s)\theta(z) + \psi_z^{Wo}(s)W^O(z) + \psi_z^{\chi o}(s)\chi^O(z). \tag{3c}$$

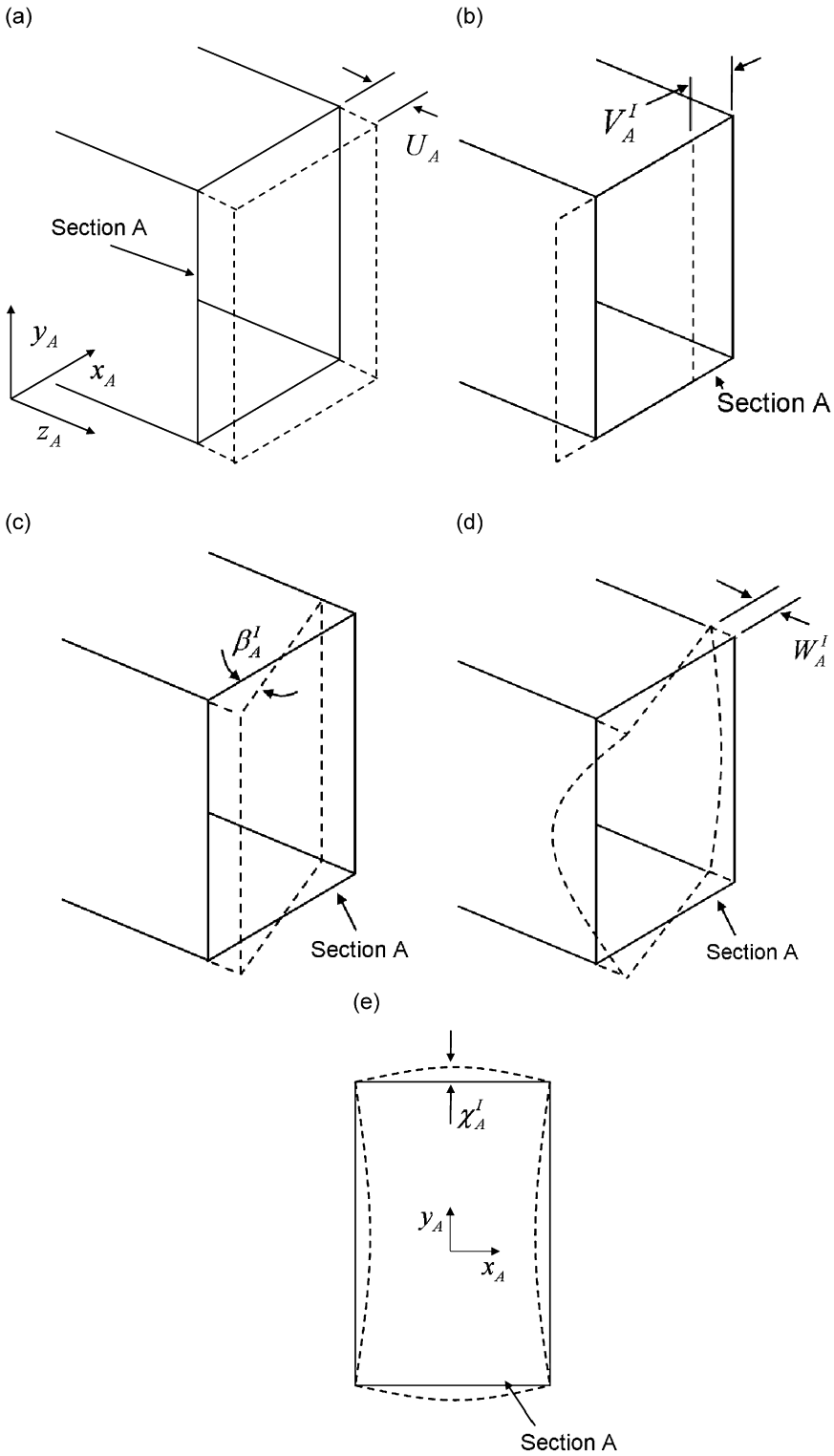

Fig. 2. Sectional displacement/deformation patterns corresponding to one-dimensional displacement measures needed to describe in-plane bending deformation of Section A in Fig. 1(b): (a) extension, (b) in-plane bending deflection, (c) in-plane bending/shear rotation, (d) in-plane bending warping, and (e) in-plane bending distortion.

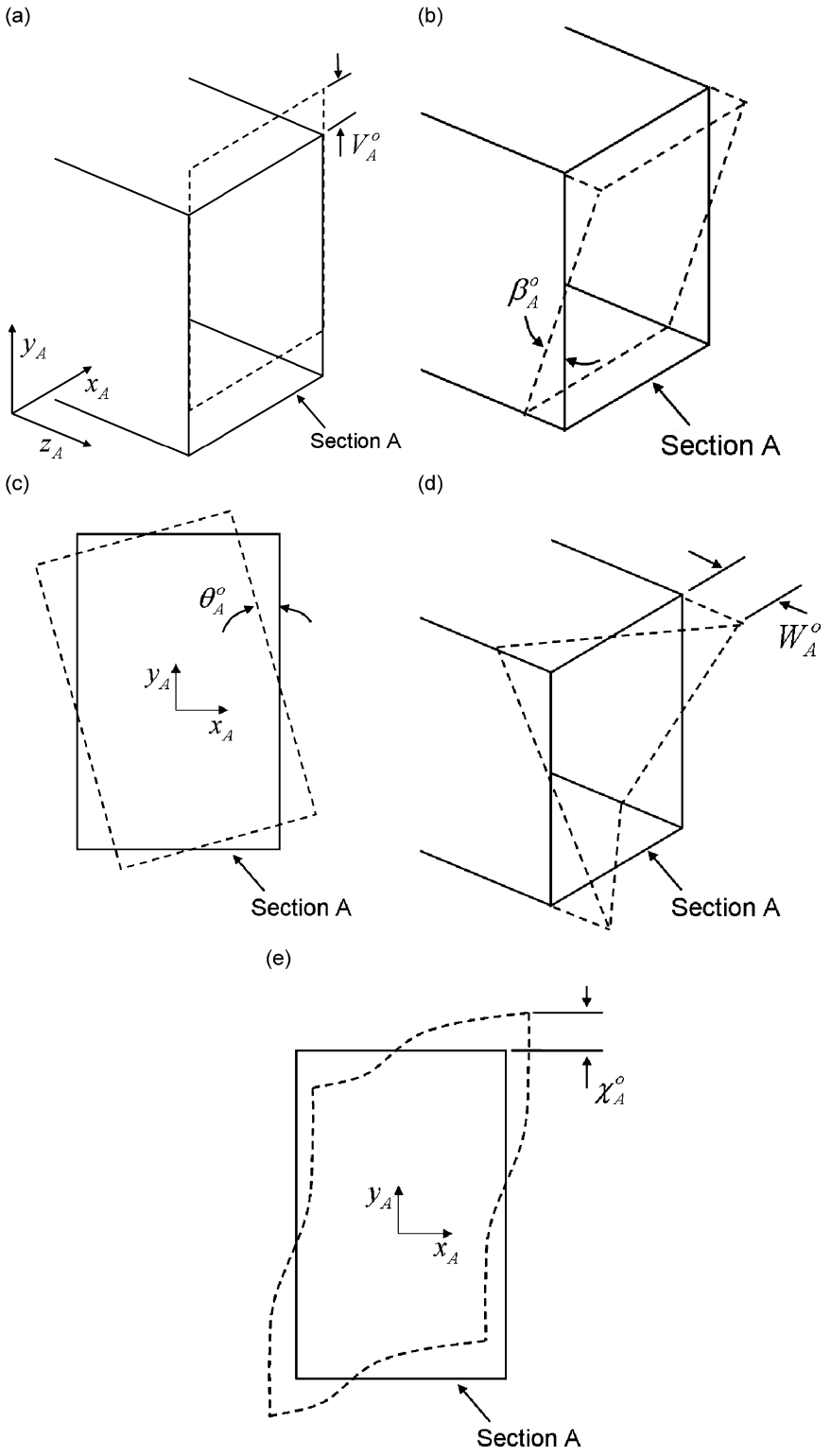

Fig. 3. Sectional displacement/deformation patterns corresponding to one-dimensional displacement measures needed to describe out-of-plane bending deformation of Section A in Fig. 1(b): (a) out-of-plane bending deflection, (b) out-of-plane bending/shear rotation, (c) torsional rotation, (d) torsional warping, and (e) torsional distortion.

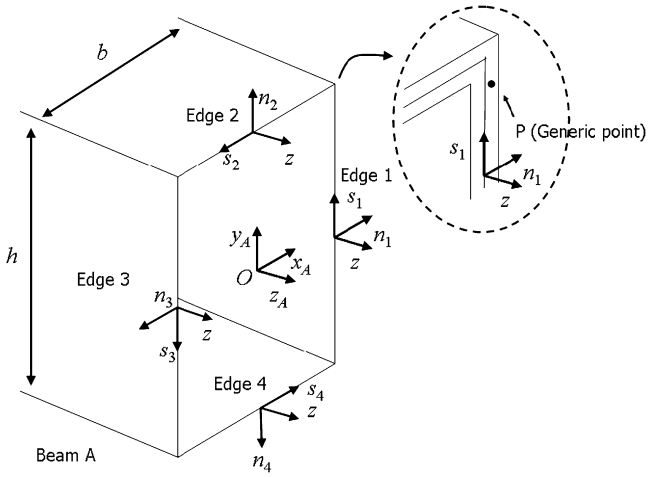

Fig. 4. Coordinates of a thin-walled box beam.

The sectional displacement patterns or the cross-section shape functions $\psi(s)$'s are illustrated in Figs. 2 and 3. By using Eqs. (1)–(3), the three-dimensional displacements of a generic point on the cross-section can be determined:

$$\tilde{u}_n(n,s,z) = u_n^I(s,z) + u_n^O(s,z), \tag{4a}$$

$$\tilde{u}_s(n,s,z) = u_s^I(s,z) + u_s^O(s,z) - n\frac{\mathrm{d}\psi_n^{\chi I}(s)}{\mathrm{d}s}\chi^I(z) - n\frac{\mathrm{d}\psi_n^{\chi o}(s)}{\mathrm{d}s}\chi^O(z), \tag{4b}$$

$$\tilde{u}_z(n,s,z) = u_z^I(s,z) + u_z^O(s,z). \tag{4c}$$

Using Eqs. (4), strains $(\varepsilon_{ss}, \varepsilon_{sz}, \varepsilon_{zz})$ can be calculated as

$$\varepsilon_{ss}(n,s,z) = -n\frac{\mathrm{d}^2\psi_n^{\chi I}(s)}{\mathrm{d}s^2}\chi^I(z) - n\frac{\mathrm{d}^2\psi_n^{\chi o}(s)}{\mathrm{d}s^2}\chi^O(z), \tag{5a}$$

$$\begin{aligned} 2\varepsilon_{sz}(n,s,z) = {} & \frac{\mathrm{d}\psi_z^U(s)}{\mathrm{d}s}U(z) + \frac{\mathrm{d}\psi_z^{\beta I}(s)}{\mathrm{d}s}\beta^I(z) + \frac{\mathrm{d}\psi_z^{WI}(s)}{\mathrm{d}s}W^I(z) \\ & + \psi_s^{VI}(s)\frac{\mathrm{d}V^I(z)}{\mathrm{d}z} - n\frac{\mathrm{d}\psi_n^{\chi I}(s)}{\mathrm{d}s}\frac{\mathrm{d}\chi^I(z)}{\mathrm{d}z} \\ & + \frac{\mathrm{d}\psi_z^{\beta o}(s)}{\mathrm{d}s}\beta^O(z) + \frac{\mathrm{d}\psi_z^{Wo}(s)}{\mathrm{d}s}W^O(z) + \psi_s^{Vo}(s)\frac{\mathrm{d}V^O(z)}{\mathrm{d}z} \\ & + \psi_s^{\theta}(s)\frac{\mathrm{d}\theta(z)}{\mathrm{d}z} + \psi_s^{\chi o}(s)\frac{\mathrm{d}\chi^O(z)}{\mathrm{d}z} - n\frac{\mathrm{d}\psi_n^{\chi o}(s)}{\mathrm{d}s}\frac{\mathrm{d}\chi^O(z)}{\mathrm{d}z}, \end{aligned} \tag{5b}$$

$$\begin{aligned} \varepsilon_{zz}(n,s,z) = {} & \psi_z^U(s)\frac{\mathrm{d}U(z)}{\mathrm{d}z} + \psi_z^{\beta I}(s)\frac{\mathrm{d}\beta^I(z)}{\mathrm{d}z} + \psi_z^{WI}(s)\frac{\mathrm{d}W^I(z)}{\mathrm{d}z} \\ & + \psi_z^{\beta o}(s)\frac{\mathrm{d}\beta^O(z)}{\mathrm{d}z} + \psi_z^{Wo}(s)\frac{\mathrm{d}W^O(z)}{\mathrm{d}z}, \end{aligned} \tag{5c}$$

where vanishing ψ terms and derivatives are omitted. Strain components not listed above are assumed to be zero. It is now straightforward to calculate stresses $(\sigma_{ss}, \sigma_{sz}, \sigma_{zz})$ from the standard constitutive relations:

$$\sigma_{ss} = \frac{E}{1-\nu^2}(\varepsilon_{ss} + \nu\varepsilon_{zz}), \quad \sigma_{zz} = \frac{E}{1-\nu^2}(\varepsilon_{zz} + \nu\varepsilon_{ss}), \quad \sigma_{sz} = 2G\varepsilon_{zs}, \tag{6}$$

where E, G and ν denote Young's modulus, the shear modulus, and Poisson's ratio of the beam, respectively.

Hamilton's principle [14] will be employed for the derivation of the finite element system equation. The Lagrangian functional of a straight thin-walled box beam $(z_1 < z < z_2)$ is defined as

$$L = T - \Pi = \frac{1}{2}\int_{z_1}^{z_2}\int_A \rho\dot{\tilde{u}}_i\dot{\tilde{u}}_i\,\mathrm{d}A\,\mathrm{d}z - \frac{1}{2}\int_{z_1}^{z_2}\int_A \sigma_{ij}\varepsilon_{ij}\,\mathrm{d}A\,\mathrm{d}z, \tag{7}$$

where ρ is a material density and $\dot{(\,)}$ denotes time derivative. In Eq. (7), T and Π are the kinetic energy and the potential energy of the system, respectively, which can be decomposed as

$$T = T^I + T^O \quad \text{and} \quad \Pi = \Pi^I + \Pi^O, \tag{8}$$

where T^I and V^I are energies induced only by in-plane bending deformation while T^O and V^O, by out-of-plane bending deformation. Coupling terms between in- and out-of-plane deformations do not appear. This decoupling can be proven by showing the following orthogonality relations between the shape functions of the in-plane (ψ^I) and out-of-plane (ψ^O) deformations:

$$\int_A \psi^I \psi^O \,\mathrm{d}A = 0, \tag{9a}$$

$$\int_A \frac{\mathrm{d}\psi^I}{\mathrm{d}s}\psi^O \,\mathrm{d}A = \int_A \psi^I \frac{\mathrm{d}\psi^O}{\mathrm{d}s}\,\mathrm{d}A = \int_A \frac{\mathrm{d}\psi^I}{\mathrm{d}s}\frac{\mathrm{d}\psi^O}{\mathrm{d}s}\,\mathrm{d}A = 0, \tag{9b}$$

$$\int_A \frac{\mathrm{d}^2\psi^{\chi I}}{\mathrm{d}s^2}\frac{\mathrm{d}^2\psi^{\chi O}}{\mathrm{d}s^2}\,\mathrm{d}A = 0. \tag{9c}$$

The dynamic solution for a thin-walled beam system minimizes the Lagrangian functional during specified time interval t_1 and t_2 [14]:

$$\begin{aligned}\delta\int_{t_1}^{t_2} L\,\mathrm{d}t &= \delta\int_{t_1}^{t_2}\left[\frac{1}{2}\int_{z_1}^{z_2}\int_A \rho\dot{\tilde{u}}_i\dot{\tilde{u}}_i\,\mathrm{d}A\,\mathrm{d}z - \frac{1}{2}\int_{z_1}^{z_2}\int_A \sigma_{ij}\varepsilon_{ij}\,\mathrm{d}A\,\mathrm{d}z\right]\mathrm{d}t\\ &= \delta\int_{t_1}^{t_2}\left[\frac{1}{2}\int_{z_1}^{z_2}\int_A (\rho\dot{\tilde{u}}_i^I\dot{\tilde{u}}_i^I + \rho\dot{\tilde{u}}_i^O\dot{\tilde{u}}_i^O)\,\mathrm{d}A\,\mathrm{d}z - \frac{1}{2}\int_{z_1}^{z_2}\int_A (\sigma_{ij}^I\varepsilon_{ij}^I + \sigma_{ij}^O\varepsilon_{ij}^O)\,\mathrm{d}A\,\mathrm{d}z\right]\mathrm{d}t = 0.\end{aligned} \tag{10}$$

In Eq. (10), the Lagrangian functional is split into in-plane terms and out-of-plane terms by use of Eq. (8). Integration-by-parts of Eq. (10) leads to

$$\delta\int_{t_1}^{t_2} L\,\mathrm{d}t = \int_{t_1}^{t_2}\left[-\int_{z_1}^{z_2}\int_A (\rho\delta\tilde{u}_i^I\ddot{\tilde{u}}_i^I + \rho\delta\tilde{u}_i^O\ddot{\tilde{u}}_i^O)\,\mathrm{d}A\,\mathrm{d}z - \int_{z_1}^{z_2}\int_A (\delta\varepsilon_{ij}^I\sigma_{ij}^I + \delta\varepsilon_{ij}^O\sigma_{ij}^O)\,\mathrm{d}A\,\mathrm{d}z\right]\mathrm{d}t = 0. \tag{11}$$

To discretize Eq. (11), the field variables are interpolated with a linear shape function matrix and a nodal displacement vector as

$$\mathbf{U}(z) = \{\mathbf{U}^I(z), \mathbf{U}^O(z)\}^{\mathrm{T}} = \{\{U, V^I, \beta^I, W^I, \chi^I\}, \{V^O, \beta^O, \theta, W^O, \chi^O\}\}^{\mathrm{T}} = [\mathbf{N}^I(z), \mathbf{N}^O(z)]\{\mathbf{d}^I, \mathbf{d}^O\}^{\mathrm{T}}. \tag{12}$$

Using Eq. (12), three-dimensional displacements in Eqs. (4) can be written as

$$\tilde{\mathbf{u}}^p = \begin{Bmatrix}\tilde{u}_n^p\\ \tilde{u}_s^p\\ \tilde{u}_z^p\end{Bmatrix} = \mathbf{\Psi}^p(n,s)\mathbf{U}^p(z) \quad (p = I \text{ or } O), \tag{13}$$

where cross-section shape function matrices $\mathbf{\Psi}^p(n,s)$ are

$$\mathbf{\Psi}^I = \begin{bmatrix} 0 & \psi_n^{VI} & 0 & 0 & \psi_n^{\chi I}\\ 0 & \psi_s^{VI} & 0 & 0 & -n\dfrac{\mathrm{d}\psi_n^{\chi I}}{\mathrm{d}s}\\ \psi_z^U & 0 & \psi_s^{\beta I} & \psi_z^{WI} & 0\end{bmatrix}, \tag{14a}$$

$$\mathbf{\Psi}^O = \begin{bmatrix} \psi_n^{Vo} & \psi_n^{\beta o} & \psi_n^{\theta} & 0 & \psi_n^{\chi o}\\ \psi_s^{Vo} & \psi_s^{\beta o} & \psi_s^{\theta} & 0 & \psi_s^{\chi o} - n\dfrac{\mathrm{d}\psi_n^{\chi o}}{\mathrm{d}s}\\ 0 & \psi_z^{\beta o} & 0 & \psi_z^{Wo} & 0\end{bmatrix}, \tag{14b}$$

where cross-section shape functions with zero values are not denoted. Using Eqs. (13) and (14), strains in Eqs. (5) can be expressed as

$$\boldsymbol{\varepsilon}^p = \begin{Bmatrix}\varepsilon_{ss}^p\\ 2\varepsilon_{sz}^p\\ \varepsilon_{zz}^p\end{Bmatrix} = \mathbf{L}^p\mathbf{N}^p\mathbf{d}^p = \mathbf{B}^p\mathbf{d}^p \quad (p = I \text{ or } O), \tag{15}$$

where the linear operator matrices are given as

$$\mathbf{L}^I = \begin{bmatrix} 0 & 0 & 0 & 0 & -n\dfrac{\mathrm{d}^2\psi_n^{\chi I}}{ds^2} \\ \dfrac{\mathrm{d}\psi_z^U}{\mathrm{d}s} & \psi_s^{VI}\dfrac{\mathrm{d}}{\mathrm{d}z} & \dfrac{\mathrm{d}\psi_z^{\beta I}}{\mathrm{d}s} & \dfrac{\mathrm{d}\psi_z^{WI}}{\mathrm{d}s} & -n\dfrac{\mathrm{d}\psi_n^{\chi I}}{\mathrm{d}s}\dfrac{\mathrm{d}}{\mathrm{d}z} \\ \psi_z^U\dfrac{\mathrm{d}}{\mathrm{d}z} & 0 & \psi_z^{\beta I}\dfrac{\mathrm{d}}{\mathrm{d}z} & \psi_z^{WI}(s)\dfrac{\mathrm{d}}{\mathrm{d}z} & 0 \end{bmatrix}, \tag{16a}$$

$$\mathbf{L}^O = \begin{bmatrix} 0 & 0 & 0 & 0 & -n\dfrac{\mathrm{d}^2\psi_n^{\chi o}}{\mathrm{d}s^2} \\ \psi_s^{Vo}\dfrac{\mathrm{d}}{\mathrm{d}z} & \dfrac{\mathrm{d}\psi_z^{\beta o}}{\mathrm{d}s} & \psi_s^{\theta}\dfrac{\mathrm{d}}{\mathrm{d}z} & \dfrac{\mathrm{d}\psi_z^{Wo}}{\mathrm{d}s} & \psi_\xi^{\chi o}\dfrac{\mathrm{d}}{\mathrm{d}z} - n\dfrac{\mathrm{d}\psi_n^{\chi o}}{\mathrm{d}s}\dfrac{\mathrm{d}}{\mathrm{d}z} \\ 0 & \psi_z^{\beta o}\dfrac{\mathrm{d}}{\mathrm{d}z} & 0 & \psi_z^{Wo}\dfrac{\mathrm{d}}{\mathrm{d}z} & 0 \end{bmatrix}. \tag{16b}$$

Substituting Eqs. (13)–(16) into Eq. (11) gives

$$\delta\int_{t_1}^{t_2} L\,\mathrm{d}t = \int_{t_1}^{t_2}[-(\delta\mathbf{d}^I)^{\mathrm{T}}\mathbf{M}^I\ddot{\mathbf{d}}^I - (\delta\mathbf{d}^O)^{\mathrm{T}}\mathbf{M}^O\ddot{\mathbf{d}}^O - (\delta\mathbf{d}^I)^{\mathrm{T}}\mathbf{K}^I\mathbf{d}^I - (\delta\mathbf{d}^O)^{\mathrm{T}}\mathbf{K}^O\mathbf{d}^O]\,\mathrm{d}t = 0, \tag{17}$$

where stiffness matrices $\mathbf{K}^p$ and mass matrices $\mathbf{M}^p$ are

$$\mathbf{M}^p = \int_{-1}^{1}\int_A (\mathbf{N}^p)^{\mathrm{T}}(\mathbf{\Psi}^p)^{\mathrm{T}}\rho\mathbf{\Psi}^p\mathbf{N}^p|J|\,\mathrm{d}A\,\mathrm{d}\xi \quad (p = I \text{ or } O) \tag{18}$$

$$\mathbf{K}^p = \int_{-1}^{1}\int_A (\mathbf{B}^p)^{\mathrm{T}}\mathbf{E}\mathbf{B}^p|J|\,\mathrm{d}A\,\mathrm{d}\xi \quad (p = I \text{ or } O) \tag{19}$$

with

$$\mathbf{E} = \begin{bmatrix} E_1 & 0 & 0 \\ 0 & G & 0 \\ 0 & 0 & E_1 \end{bmatrix}. \tag{20}$$

In the above, $E_1 = E/(1-\nu^2)$ and the Jacobian $|J|$ is the half of the element length. In Appendix A, explicit forms of $\mathbf{K}^p$ and $\mathbf{M}^p$ are listed.

The final forms of the system equation from Eq. (17) for modal analysis can be written as

$$\mathbf{K}^p\hat{\mathbf{d}}^p = \omega^2\mathbf{M}^p\hat{\mathbf{d}}^p \quad (p = I \text{ or } O), \tag{21}$$

where $\hat{\mathbf{d}}^p = \mathbf{d}^p\,\mathrm{e}^{\mathrm{j}\omega t}$ (ω: angular frequency).

3. Joint interface conditions

If two box beams meet at an angled joint in the same plane as depicted in Fig. 1, no coupling between in-plane and out-of-plane deformations occurs due to the angled joint connection. In this case, the joint interface condition derived for static problems [12,13] can be used for the present dynamic problems to match field variables of Beam A and Beam B in Fig. 1 at an angled joint. Fig. 1(b) illustrates a top view of the joint model employed here. Two straight beams are assumed to meet at an angle of 2ϕ sharing the edge $\overline{QQ}'$. For the field variables $(U, V^I, \beta^I, V^O, \beta^O, \theta)$ having no cross-sectional deformation, the relation between the variables of Beam A and those of Beam B can be found simply by the standard vector calculus because they are associated with non-self-equilibrated force resultants. However, it is not possible to use the same procedure for warping and distortion deformations because the corresponding force resultants are self-equilibrated. Therefore, one may simply assume that

$$W_A^p = W_B^p \quad \text{and} \quad \chi_A^p = \chi_B^p \quad (p = I \text{ or } O). \tag{22}$$

If Eq. (22) is used, the deformations due to W and χ are completely decoupled from cross-sectional deformations resulting from other field variables such as U, V^I, etc.; flexibility due to the existence of an angled joint cannot be accounted for and the resulting solution will behave almost similarly to that by the Timoshenko beam theory.

A remedy to fix the above-mentioned defect is to minimize the difference between three-dimensional displacements due to the field variables of Beam A and those of Beam B on an imaginary Joint Section J in Fig. 1(b). According to Jang et al. [12] and Jang and Kim [13], the following minimization problem is set up:

$$\text{Find } \mathbf{T}_{AB}^p \in \mathbb{R}^{5\times 5} \quad \text{for} \quad \mathbf{U}_A^p = \mathbf{T}_{AB}^p\mathbf{U}_B^p \quad (p = I \text{ or } O) \tag{23a}$$

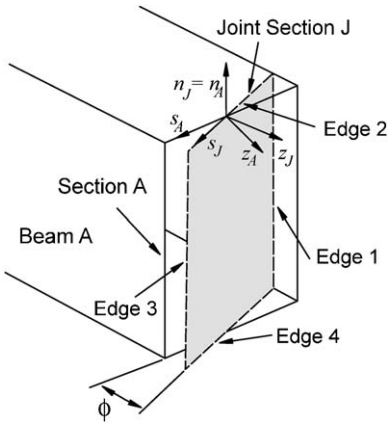

Fig. 5. Joint coordinates (n_J, s_J, z_J) on Edge 2 of Joint Section J (edge index numbers are skipped).

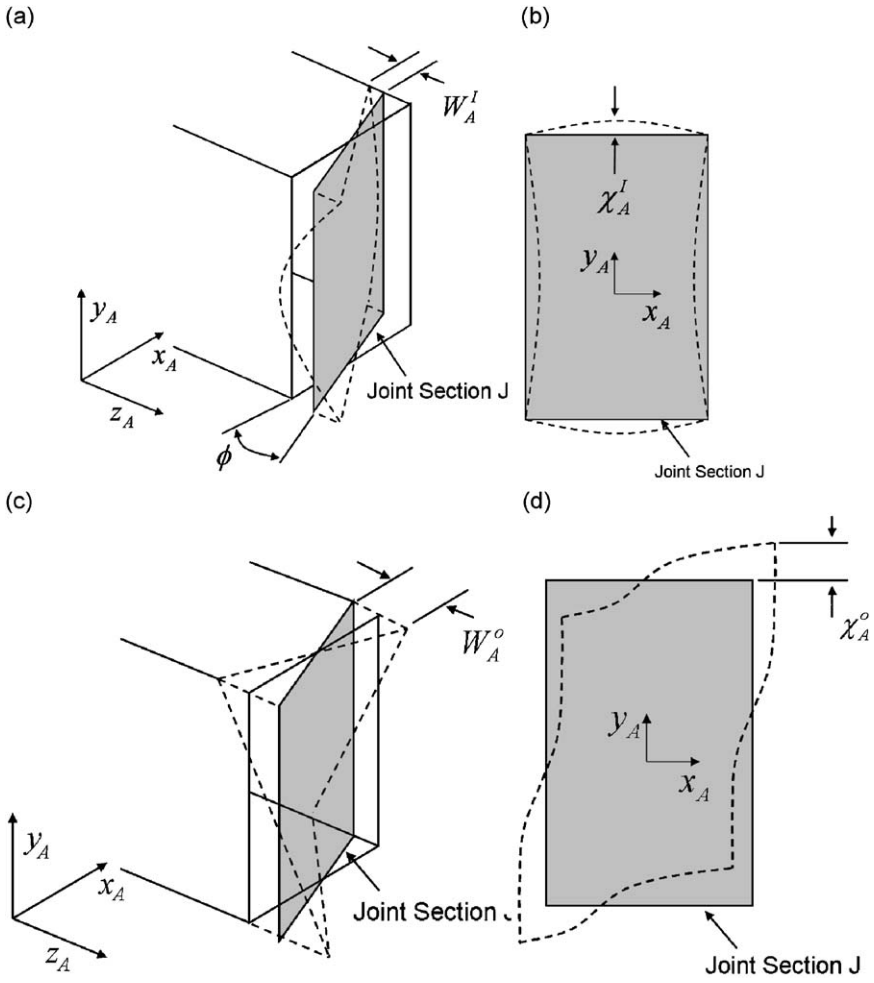

Fig. 6. Displacement/deformation patterns on Joint Section J due to deformations on Section A: (a) in-plane bending warping, (b) in-plane bending distortion, (c) out-of-plane torsional warping, and (d) out-of-plane torsional distortion.

$$\text{minimizing } \widehat{\Pi}(\mathbf{U}_A^p, \mathbf{U}_B^p) \text{ for any admissible } \mathbf{U}_A^p \text{ (or } \mathbf{U}_B^p), \tag{23b}$$

where

$$\widehat{\Pi}^p(\mathbf{U}_A^p, \mathbf{U}_B^p) = \int_{n_J}\int_{s_J} ||\tilde{\mathbf{u}}_{A_J}^p(s_J, n_J) - \tilde{\mathbf{u}}_{B_J}^p(s_J, n_J)||^2 \, \mathrm{d}s_J \, \mathrm{d}n_J, \tag{23c}$$

and

$$\mathbf{U}_q^I = \{U_q, V_q^I, \beta_q^I, W_q^I, \chi_q^I\}^{\mathrm{T}} \quad (q = A \text{ or } B), \tag{23d}$$

$$\mathbf{U}_q^O = \{V_q^O, \beta_q^O, \theta_q, W_q^O, \chi_q^O\}^{\mathrm{T}} \quad (q = A \text{ or } B). \tag{23e}$$

In Eq. (23c), $\tilde{\mathbf{u}}_{A_J}^p$ and $\tilde{\mathbf{u}}_{B_J}^p$ ($p = I$ or O) denote three-dimensional displacements on Joint Section J due to deformations by $\mathbf{U}_A^p$ at Section A and deformations $\mathbf{U}_B^p$ at Section B, respectively. To express $\tilde{\mathbf{u}}_{A_J}^p$ and $\tilde{\mathbf{u}}_{B_J}^p$, new coordinates n_J and s_J are defined on Joint Section J (see Fig. 5). By minimizing the difference between three-dimensional displacements on Joint Section J in Eq. (23c), the transformation relations $\mathbf{T}_{AB}^p$ for in- and out-of-plane field variables can be found. Note that two sets of decoupled minimization problems are solved for $\mathbf{T}_{AB}^I$ and $\mathbf{T}_{AB}^O$.

In making use of Eqs. (23), the most important issue is how to evaluate $\tilde{\mathbf{u}}_{A_J}^p$ and $\tilde{\mathbf{u}}_{B_J}^p$ on Joint Section J from $\mathbf{U}_A^p$ and $\mathbf{U}_B^p$, the deformations defined on different sections, Sections A and B. Therefore, physics-based kinematic assumptions used to relate $\mathbf{U}_A^p$ (or $\mathbf{U}_B^p$) and the deformations on Joint Section J must be found. For the field variables (U, V^I, β^I) and (V^O, β^O, θ) associated with sectional rigid-body motions, the transfer relations between field variables on Section A and those on Joint Section J are easy to find. By using the vector calculus of rigid-body motions, one can write

$$\begin{Bmatrix} U \\ V^I \\ \beta^I \end{Bmatrix}_{A_J} = \begin{bmatrix} \cos\phi & -\sin\phi & 0 \\ \sin\phi & \cos\phi & 0 \\ 0 & 0 & 1 \end{bmatrix} \begin{Bmatrix} U \\ V^I \\ \beta^I \end{Bmatrix}_{A}, \tag{24a}$$

Table 1
Calculated eigenfrequencies of the box beam in Fig. 1 for $2\phi = 30^\circ$ (unit: Hz).

Mode	Dominant mode	Shell (ANSYS)	Proposed beams	Timoshenko beams
1	First in-plane flexure mode	82.72	81.17 (−1.9%)	98.26
2	First out-of-plane rotation mode	209.59	203.25 (−3.0%)	311.95
3	Second in-plane flexure mode	258.74	278.28 (7.6%)	279.76
4	Second out-of-plane rotation mode	410.80	420.72 (2.4%)	637.19
5	Third in-plane flexure mode	417.29	437.99 (5.0%)	496.08
6	Coupled out-of-plane flexure and rotation mode	440.11	461.77 (4.9%)	459.30
7	Coupled out-of-plane distortion and warping mode	500.91	507.48 (1.3%)	–
8	Coupled out-of-plane distortion and warping mode	503.78	507.50 (0.7%)	–
9	Coupled out-of-plane distortion and warping mode	553.55	555.99 (0.4%)	–
10	Coupled out-of-plane distortion and warping mode	615.34	635.26 (3.2%)	–

Table 2
Calculated eigenfrequencies of the box beam in Fig. 1 for $2\phi = 60^\circ$ (unit: Hz).

Mode	Dominant mode	Shell (ANSYS)	Proposed beams	Timoshenko beams
1	First in-plane flexure mode	71.85	70.54 (−1.8%)	87.82
2	First out-of-plane rotation mode	228.43	212.93 (−6.8%)	451.46
3	Second in-plane flexure mode	262.82	282.79 (7.6%)	284.29
4	Third in-plane flexure mode	367.00	384.20 (4.7%)	443.70
5	Coupled out-of-plane flexure and rotation mode	408.77	414.66 (1.4%)	454.30
6	Coupled out-of-plane flexure and rotation mode	445.96	464.97 (4.3%)	–
7	Second out-of-plane rotation mode	503.57	507.90 (0.9%)	636.50
8	Coupled out-of-plane distortion and warping mode	511.09	516.25 (1.0%)	–
9	Coupled out-of-plane distortion and warping mode	554.92	559.37 (0.8%)	–
10	Coupled out-of-plane distortion and warping mode	624.23	651.49 (4.4%)	–

$$\begin{Bmatrix} V^O \\ \beta^O \\ \theta \end{Bmatrix}_{A_J} = \begin{bmatrix} 1 & 0 & 0 \\ 0 & \cos\phi & -\sin\phi \\ 0 & \sin\phi & \cos\phi \end{bmatrix} \begin{Bmatrix} V^O \\ \beta^O \\ \theta \end{Bmatrix}_{A}. \tag{24b}$$

The positive directions of $(\,)_{A_J}$ are based on the joint coordinate systems (n_J, s_J, z_J). For example, in Fig. 5, if $U_{A_J} > 0$, the Joint Section J moves in the $+z_J$ direction, and if $V^I_{A_J} > 0$, the Joint Section J moves in the $+s_J$ direction.

Table 3
Calculated eigenfrequencies of the box beam in Fig. 1 for $2\phi = 90^\circ$ (unit: Hz).

Mode	Dominant mode	Shell (ANSYS)	Proposed beams	Timoshenko beams
1	First in-plane flexure mode	62.68	61.47 (−1.9%)	77.65
2	First out-of-plane rotation mode	234.96	217.03 (−7.6%)	442.18
3	Second in-plane flexure mode	271.83	292.88 (7.7%)	294.41
4	Third in-plane flexure mode	342.26	354.93 (3.7%)	410.42
5	Coupled out-of-plane flexure and rotation mode	394.31	402.15 (2.0%)	–
6	Coupled out-of-plane flexure and rotation mode	453.98	470.41 (3.6%)	–
7	Second out-of-plane rotation mode	503.09	508.98 (1.2%)	531.51
8	Coupled out-of-plane distortion and warping mode	513.97	518.30 (0.8%)	–
9	Coupled out-of-plane distortion and warping mode	555.14	560.10 (0.9%)	–
10	Coupled out-of-plane distortion and warping mode	625.96	656.09 (4.8%)	–

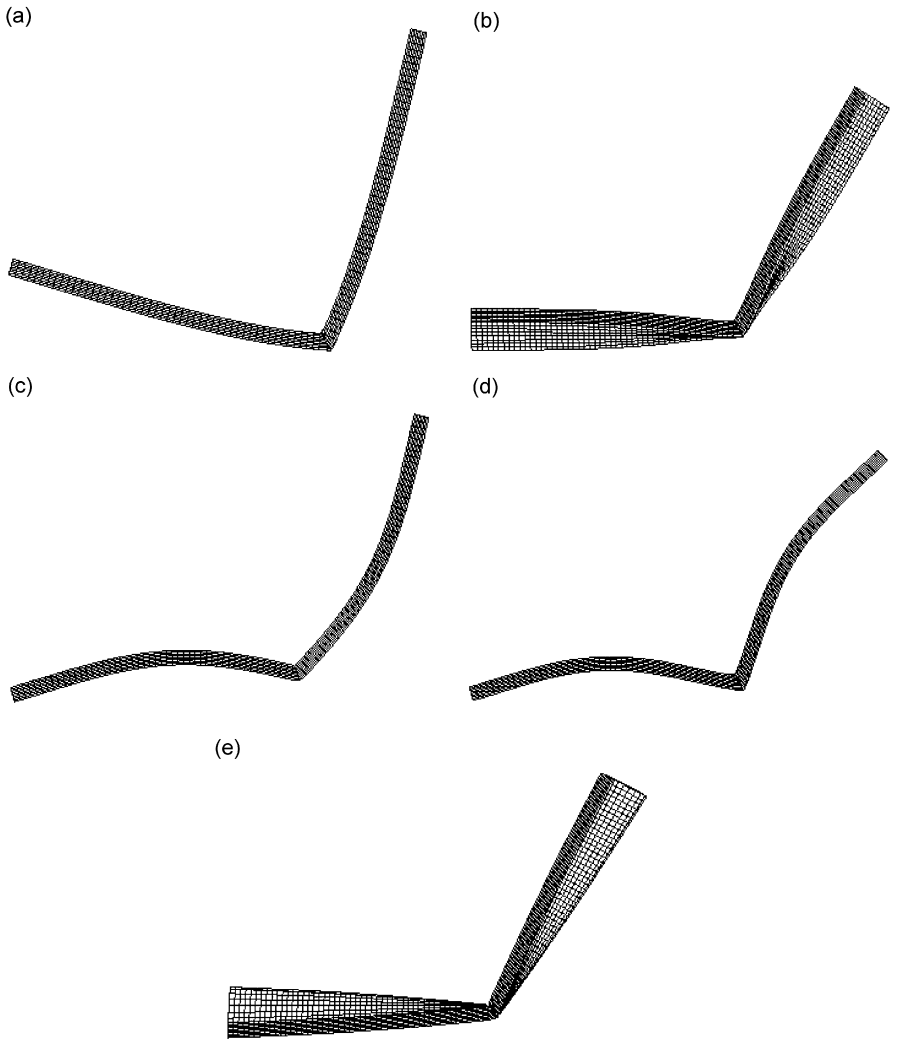

Fig. 7. Eigenmode shapes of the thin-walled box beam in Fig. 1 ($2\phi = 60^\circ$) by the developed higher-order beam analysis: (a) first in-plane flexure, (b) first out-of-plane torsional rotation, (c) second in-plane flexure, (d) third in-plane flexure, and (e) second out-of-plane torsional rotation.

In finding the relation between $(W^p_{A_J}, \chi^p_{A_J})$ and $\mathbf{U}^p_A$ $(p = I \text{ or } O)$, we note that no additional elastic strain energy should be stored in the region between Section A and Joint Section J if the transfer relation is correct. To satisfy this condition, the displacements of all points lying on the edges of Joint Section J are exactly the same as those of their corresponding points on Section A. This also means that all points lying on the same z_A-axis between Section A and Joint Section J should have the same displacements. Fig. 6 illustrates the deformation patterns of Joint Section J by warping and distortion of Section A based on this kinematic assumption. The comparison of the sectional deformations of Section A in Fig. 2(d, e) and Fig. 3(d, e) and those in Fig. 6 will clearly demonstrate how the displacements on Joint Section J occur due to (W^p_A, χ^p_A).

The transfer relation between Section A and Joint Section J equally applies in establishing the transfer relation between Section B and Joint Section J. One can then immediately see the mismatch in the displacements on Joint Section J whenever the joint angle 2ϕ is not zero. To minimize the displacement mismatch on Joint Section J, other field variables such as U, V^I, β^I, V^O, β^O and θ should interact with W^p and χ^p $(p = I \text{ or } O)$, which results in the coupling among all field variables.

Employing the above kinematic relations, the three-dimensional displacement $\tilde{\mathbf{u}}^p_{A_J}$ $(p = I \text{ or } O)$ on Edge 1 of Joint Section J can be written in terms of $\mathbf{U}^I_A$ and $\mathbf{U}^O_A$ as

- for in-plane deformation

$$ {}^1\tilde{u}^I_{A_J,n_J}(n_J, s_J) = -U_A \sin\phi - V^I_A \cos\phi + \psi^{\chi I}_n \chi^I_A \cos\phi - \psi^{WI}_z W^I_A \sin\phi, \tag{25a} $$

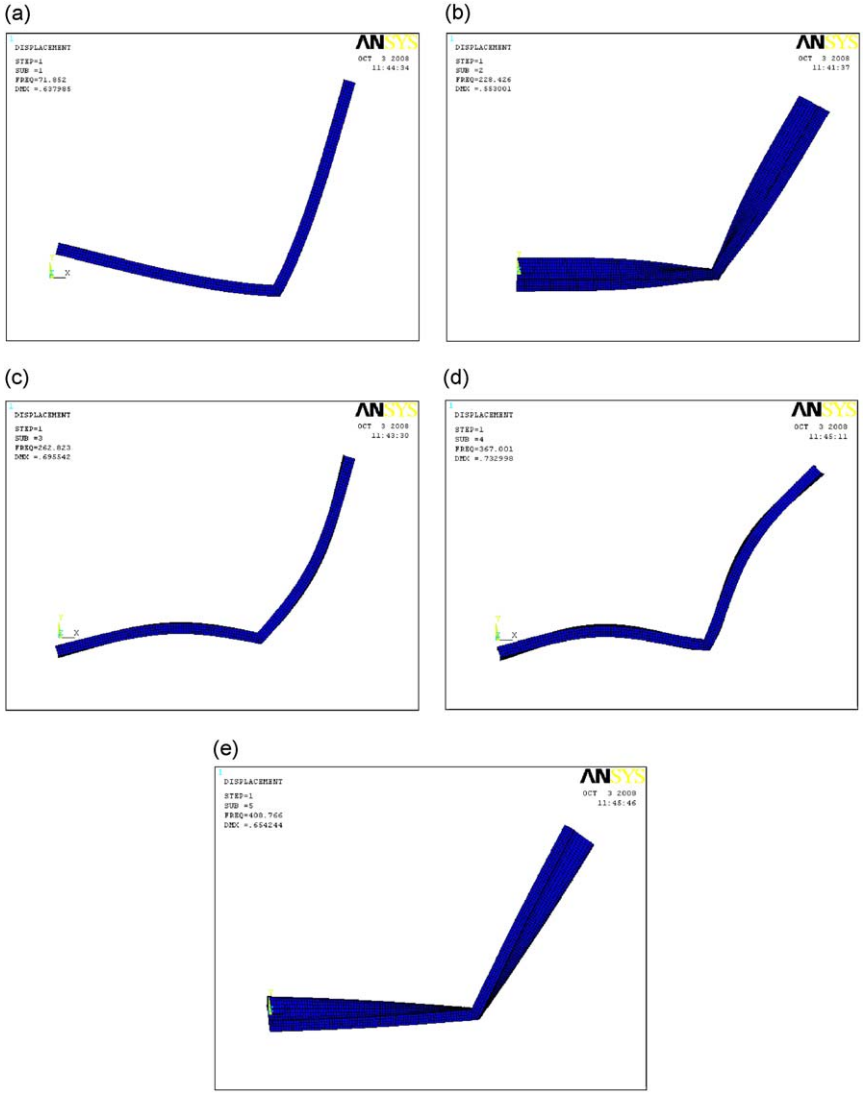

Fig. 8. Eigenmode shapes of the thin-walled beam in Fig. 1 ($2\phi = 60^\circ$) by the ANSYS shell analysis: (a) first in-plane flexure, (b) first out-of-plane torsional rotation, (c) second in-plane flexure, (d) third in-plane flexure, and (e) second out-of-plane torsional rotation.

$$ {}^1\tilde{u}^I_{A_J,s_J}(n_J,s_J) = -n_J \frac{\mathrm{d}\psi^{\chi I}_n}{\mathrm{d}s}\chi^I_A, \tag{25b} $$

$$ {}^1\tilde{u}^I_{A_J,z_J}(n_J,s_J) = U_A\cos\phi - V^I_A\sin\phi - \frac{b}{2}\beta^I_A + \psi^{\chi I}_n\chi^I_A\sin\phi + \psi^{WI}_z W^I_A\cos\phi, \tag{25c} $$

and

- for out-of-plane deformation

$$ {}^1\tilde{u}^O_{A_J,n_J}(n_J,s_J) = -s_J\beta^O_A\sin\phi - s_J\theta_A\cos\phi - \frac{b}{2}s_J W^O_A\sin\phi + \psi^{\chi o}_n\chi^O_A\cos\phi, \tag{26a} $$

$$ {}^1\tilde{u}^O_{A_J,s_J}(n_J,s_J) = V^O_A + \frac{b}{2}\beta^O_A\sin\phi + \frac{b}{2}\theta_A\cos\phi + \frac{bh}{b+h}\chi^O_A - n_J\frac{\mathrm{d}\psi^{\chi o}_n}{\mathrm{d}s}\chi^O_A, \tag{26b} $$

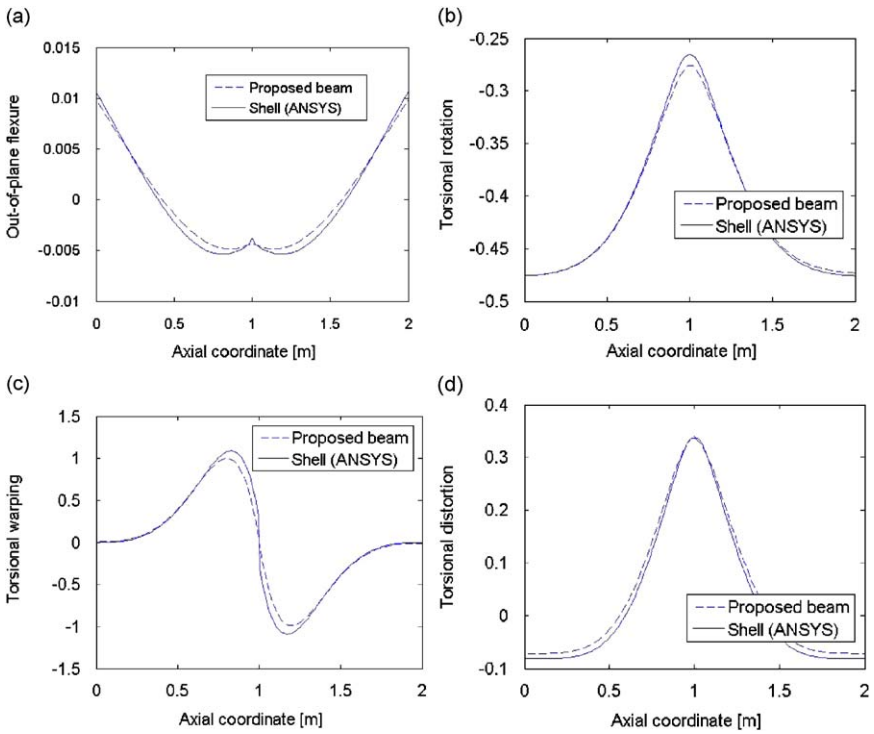

Fig. 9. Distributions of one-dimensional field variables for the second modes in Figs. 6(b) and 7(b) (the angled joint is located at $z = 1$): (a) V^O (out-of-plane bending deflection), (b) θ (torsional rotation), (c) W^O (torsional warping), and (d) χ^O (torsional distortion).

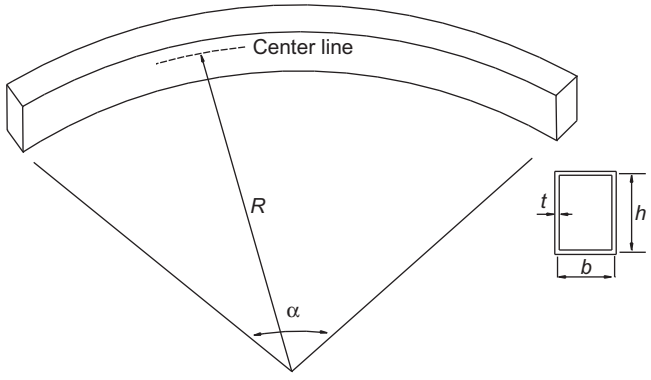

Fig. 10. A curved thin-walled beam ($R = 1000$ mm, $\alpha = 90^\circ$, $b = 50$ mm, $h = 70$ mm, $t = 1$ mm, $E = 200$ GPa, and $v = 0.3$).

Table 4
Calculated eigenfrequencies of the curved beam in Fig. 10 (unit: Hz).

Mode	Dominant mode	Shell (ANSYS)	Proposed beams	Timoshenko beams
1	First in-plane flexure mode	111.43	117.47 (5.4%)	148.46
2	First out-of-plane rotation mode	239.31	239.00 (−0.1%)	442.41
3	Second out-of-plane rotation mode	261.21	259.52 (−0.6%)	542.46
4	Second in-plane flexure mode	298.55	317.16 (6.2%)	412.87
5	Coupled out-of-plane distortion and warping mode	372.70	369.78 (−0.8%)	–
6	Third out-of-plane rotation mode	416.32	415.86 (−0.1%)	–
7	Third in-plane flexure mode	508.03	533.19 (5.0%)	796.63
8	Coupled out-of-plane distortion and warping mode	570.39	585.86 (2.7%)	–
9	Fourth in-plane flexure mode	647.44	640.37 (−1.1%)	–
10	Fifth in-plane flexure mode	700.45	674.28 (−3.7%)	–

$$ {}^1\tilde{u}^O_{A_J,z_J}(n_J,s_J) = s_J\beta^O_A \cos\phi - s_J\theta_A \sin\phi + \frac{b}{2}s_J W^O_A \cos\phi + \psi^{\chi o}_n \chi^O_A \sin\phi. \tag{26c} $$

Because Joint Section J can be regarded as a rotated section of Section A or Section B, its size is assumed to be $b \times h$ [13]. For instance, ${}^1\tilde{u}^I_{A_J,z_J}$ in the direction of z_J by β^I_A becomes $-b/2\beta^I_A$ as given in Eq. (25c). As seen in Eqs. (25a) and (25c), the axial displacement by warping of Section A induces normal displacement as well as axial displacement on Joint Section J. Likewise, the normal displacement $\psi^{\chi I}_n \chi^I_A$ of distortion of Section A induces axial and normal displacements on Joint Section J.

The three-dimensional displacements $\tilde{\mathbf{u}}^p_{A_J}$ ($p = I$ or O) on the other edges are listed in Appendix A. Three-dimensional displacements $\tilde{\mathbf{u}}^p_{B_J}$ on Section B can be obtained by putting $-\phi$ instead of ϕ in Eqs. (25) and (26) and those in Appendix A. For example,

$$ {}^1\tilde{u}^I_{B_J,n_J}(n_J,s_J) = U_B \sin\phi - V^I_B \cos\phi + \psi^{\chi I}_n \chi^I_B \cos\phi + \psi^{WI}_z W^I_B \sin\phi. \tag{27} $$

Since the three-dimensional displacements on Joint Section J are expressed in terms of $\mathbf{U}^I_A$, $\mathbf{U}^O_A$, $\mathbf{U}^I_B$ and $\mathbf{U}^O_B$, the functional $\widehat{\Pi}^p$ ($p = I$ or O) representing the difference between displacements of Beam A and Beam B on Joint Section J can be also written in terms of these field variables. Considering the minimization of $\widehat{\Pi}^p$ with respect to arbitrary configuration of $\mathbf{U}^p_A$,

$$ \frac{\partial\widehat{\Pi}^I}{\partial\zeta^I_A} = 0 \quad (\zeta^I_A = U_A, V^I_A, \beta^I_A, W^I_A \text{ and } \chi^I_A), \tag{28a} $$

and

$$ \frac{\partial\widehat{\Pi}^O}{\partial\zeta^O_A} = 0 \quad (\zeta^o_A = V^O_A, \beta^O_A, \theta, W^O_A \text{ and } \chi^O_A). \tag{28b} $$

Because $\widehat{\Pi}^p$ in Eq. (23c) is quadratic with respect to the field variables, Eqs. (28) yield linear relations between the field variables, which can be symbolically written as

$$ \mathbf{T}^p_A\mathbf{U}^p_A + \mathbf{T}^p_B\mathbf{U}^p_B = 0 \quad (p = I \text{ or } O), \tag{29} $$

where the components of the coefficient matrices $\mathbf{T}^p_A$ and $\mathbf{T}^p_B$ consist of nonlinear combinations of section geometric parameters and the joint angle. The matrices $\mathbf{T}^p_{AB}$ in Eq. (23a) are given by

$$ \mathbf{T}^p_{AB} = -(\mathbf{T}^p_A)^{-1}\mathbf{T}^p_B \quad (p = I \text{ or } O). \tag{30} $$

In this work, the symbolic expression function of Matlab [15] is used to derive $\mathbf{T}^p_{AB}$.

4. Numerical examples

4.1. A one-angled-joint thin-walled box beam structure

A thin-walled box beam structure having an angled joint of Fig. 1(a) is analyzed. The geometries and material properties of Beam A and Beam B are length = 1000 mm, $b = 50$ mm, $h = 100$ mm, $t = 2$ mm, E (Young's modulus) = 200 GPa and v (Poisson's ratio) = 0.3. To check solution accuracy, the results by the developed higher-order beam analysis are compared with those by the shell finite elements of commercial software, ANSYS [16]. The results by the Timoshenko beam theory are

also presented to see the effect of warping and distortion deformations on the flexibility of the structure. For the analysis, 100 beam elements are used both for the higher-order and Timoshenko beam analyses. Tables 1–3 list the eigenfrequencies obtained by using the higher-order beam elements, the Timoshenko beam elements, and shell elements for joint angles 2ϕ equal to 30°, 60°, and 90°. The mode shapes by the present higher-order beam analysis and those by the shell analysis are compared in Figs. 7 and 8.

From Table 1, one can see that the fundamental eigenfrequency corresponding to a dominant in-plane flexure mode by the proposed higher-order beam approach is almost identical to the result by shell elements. In the table, the numbers in

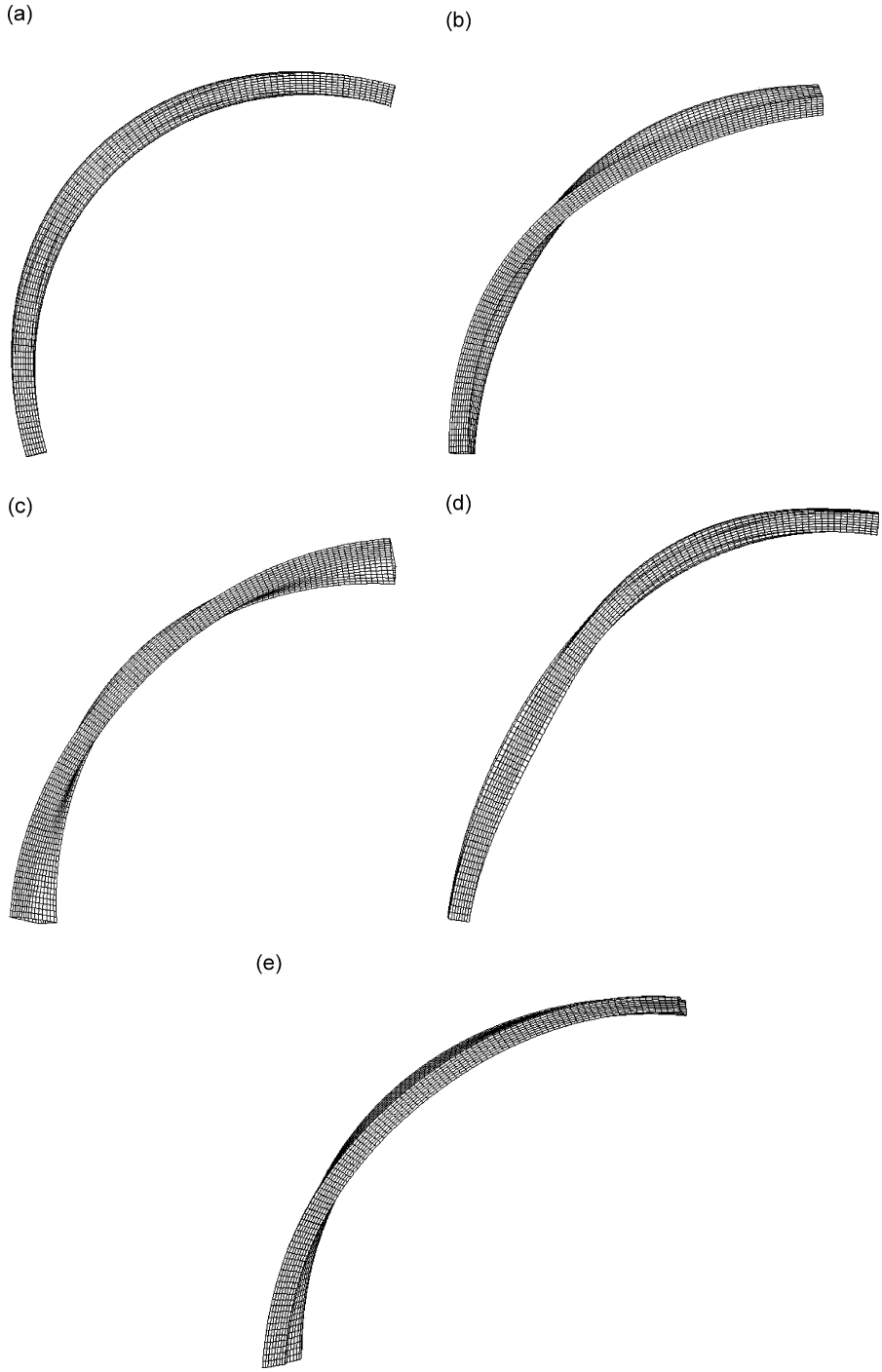

Fig. 11. Eigenmode shapes of the curved thin-walled beam in Fig. 9 by the proposed higher-order beam analysis: (a) first in-plane flexure, (b) first out-of-plane torsional rotation, (c) second out-of-plane torsional rotation, (d) second in-plane flexure, and (e) third out-of-plane torsional rotation.

parentheses denote the relative differences of the present results to those by the shell analysis. On the other hand, the Timoshenko beam analysis predicts considerably stiff behavior because the effects of cross-sectional deformations are neglected. Furthermore, the eigenmode sequence from the lowest energy mode to higher modes is incorrectly estimated by the Timoshenko theory. For instance, the Timoshenko beam analysis incorrectly predicts that the first out-of-plane rotation mode is a higher energy mode than the second in-plane flexure mode. This is due to the fact that the Timoshenko beam analysis is incapable of predicting the eigenmodes mainly consisting of cross-sectional deformations (see, e.g., from the seventh to the tenth modes in Table 1).

Let us examine the detailed mode shapes obtained by the present higher-order beam analysis and the ANSYS shell analysis. Fig. 7 shows the mode shapes by the present analysis for the case of $2\phi = 60^\circ$, which are virtually identical to those by the shell analysis in Fig. 8. The first out-of-plane torsional rotation mode shown in Figs. 7(b) and 8(b) exhibits symmetric rotation with respect to the angled joint along two connected beams while the second out-of-plane torsional rotation mode in Figs. 7(e) and 8(e) exhibits anti-symmetric rotation. The distribution of the one-dimensional field variables such as V^O, θ, W^O and χ^O are plotted as the functions of the axial coordinate in Fig. 9. It shows that the solutions by the higher-order beam analysis agree well with those by the shell analysis.

4.2. A curved thin-walled beam

The vibration analysis of a curved thin-walled beam in Fig. 10 is carried out. The beam is modeled by straight thin-walled box beam elements connected at angled joints. For the finite element discretization, 100 higher-order straight beam elements are employed, each of which is connected to adjacent elements at the same angle of $2\phi = 0.9^\circ$. Earlier, this problem is solved by using curved higher-order beam elements [17,18].

Table 4 lists the eigenfrequencies by the higher-order beam, Timoshenko beam and shell theories. It is apparent from Table 4 that the difference between the higher-order beam results and the shell results is marginal. As was expected, not only the values of the eigenfrequencies but also the mode sequence is incorrectly predicted if the Timoshenko beam theory neglecting warping and distortion is used. Significant effects of cross-sectional deformations can be seen in Fig. 11.

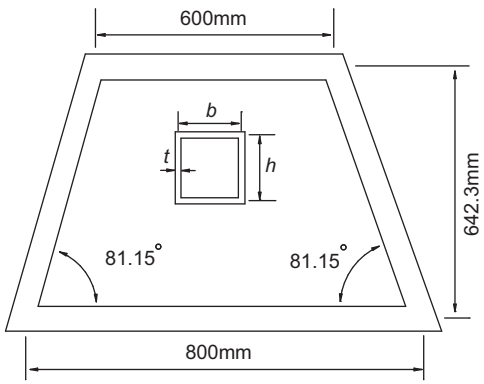

Fig. 12. A closed-loop thin-walled box beam structure ($b = 50$ mm, $h = 50$ mm, $t = 2$ mm, $E = 200$ GPa, and $\nu = 0.3$).

Table 5
Calculated eigenfrequencies of the closed-loop frame structure in Fig. 11 (unit: Hz).

Mode	Dominant mode	Shell (ANSYS)	Proposed beams	Timoshenko beams
1	First out-of-plane flexure and rotation mode	97.18	91.98 (−5.3%)	172.89
2	First in-plane flexure mode	182.12	183.24 (0.6%)	213.89
3	Second out-of-plane flexure and rotation mode	319.56	336.23 (5.2%)	342.96
4	Second in-plane flexure mode	330.11	346.13 (4.9%)	349.92
5	Third out-of-plane flexure and rotation mode	510.60	544.92 (6.7%)	585.38
6	Third in-plane flexure mode	538.71	559.16 (3.8%)	597.96
7	Fourth out-of-plane flexure and rotation mode	588.34	584.32 (−0.7%)	669.10
8	Fifth out-of-plane flexure and rotation mode	592.20	611.52 (3.3%)	823.69
9	Fourth in-plane flexure mode	649.60	663.00 (2.1%)	719.49
10	Fifth in-plane flexure mode	747.47	718.96 (−3.8%)	842.03

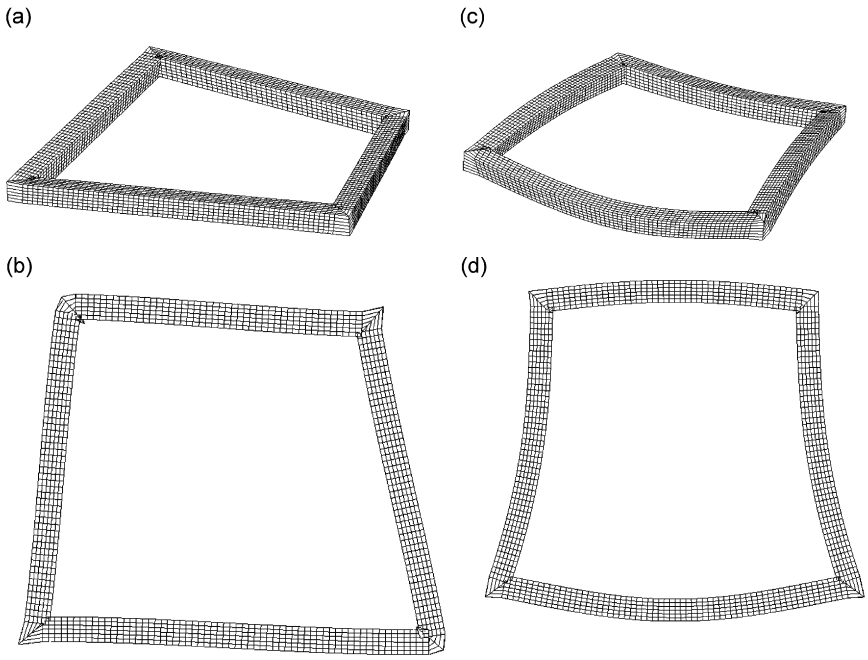

Fig. 13. Eigenmode shapes of the thin-walled structure in Fig. 11 by the proposed higher-order beam analysis: (a) first out-of-plane flexure and torsional rotation, (b) first in-plane flexure, (c) second out-of-plane flexure and torsional rotation, and (d) second in-plane flexure.

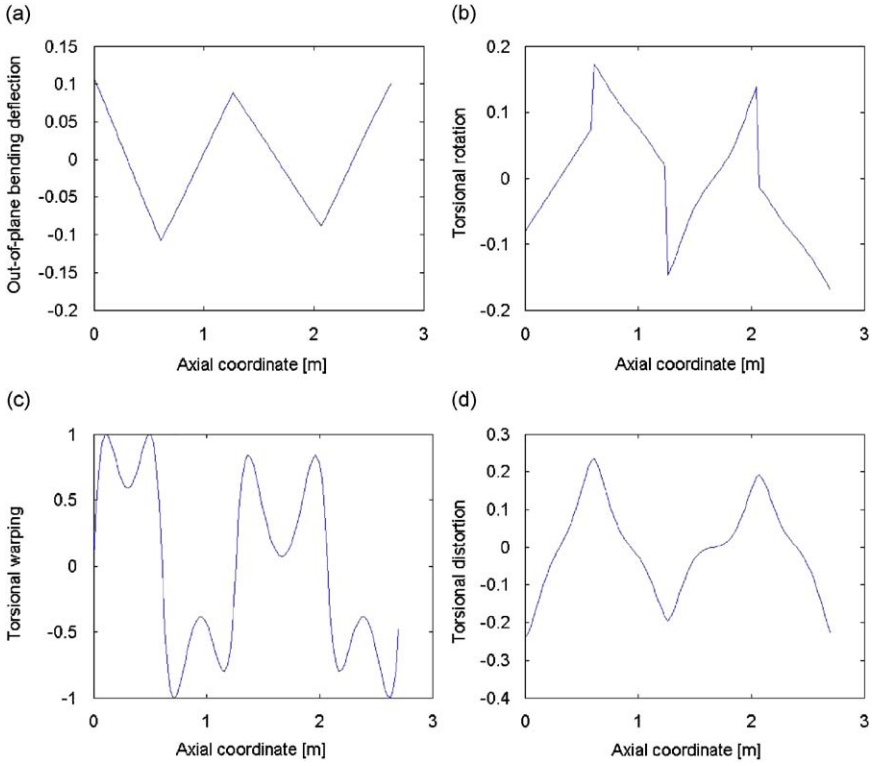

Fig. 14. Distributions of one-dimensional field variables for the first mode in Fig. 12(a): (a) V^O (out-of-plane bending deflection), (b) θ (torsional rotation), (c) W^O (torsional warping), and (d) χ^O (torsional distortion). The axial coordinate is measured counterclockwise starting from the top right corner of the structure.

4.3. A closed-loop thin-walled box beam structure

Fig. 12 illustrates a closed-loop thin-walled structure consisting of four straight thin-walled box beams. This layout is efficient in supporting out-of-plane directional loads, and thus popularly used in many frame structures such as the sub-frame of a car. Note that the proposed joint match condition is applicable for joints with acute angles. Table 5 lists the eigenfrequencies of the structure. Unlike the previous open-loop beam structures, as can be seen in Fig. 13, eigenmodes involving significant cross-sectional deformations are difficult to appear because there is no open end. Therefore, most of the fundamental modes can be predicted by the Timoshenko theory. Nevertheless, there are still serious defects in the prediction by the Timoshenko theory. Most of all, the first eigenfrequency by the Timoshenko theory is too high; it is almost twice as high as that calculated by the shell or the higher-order beam analysis. This inaccuracy results from ignorance of cross-sectional deformations due to warping and distortion. As shown in Fig. 14, torsional warping and distortional deformations cannot be ignored even in the lowest eigenmode. When higher eigenfrequencies are calculated, the Timoshenko beam theory performs better, but there is a situation where the mode sequence is incorrectly estimated.

5. Conclusions

The vibration analysis of a thin-walled beam structure having angled joints was carried out by using a higher-order beam theory. The main contributions of this work are (1) that the beam-based vibration analysis of boxed beams joined at an angle is accomplished without using artificial joint elements while existing beam-based approaches should employ special additional joint elements and (2) that the solutions obtained by the developed analysis technique compare favorably with the solutions by the detailed shell analysis.

Unlike the Timoshenko-kinematics-based beam approach, the present higher-order beam approach calculated the eigenfrequencies of thin-walled box beam systems only in marginal errors and also predicted the modal order correctly. Even in thin-walled box beam systems without any open end, the cross-sectional warping and distortional deformations affected the lowest eigenfrequencies significantly. The effects of the sectional deformations were accurately modeled in the developed approach. The developed beam analysis required the use of more dof in the higher-order beam theory than those of the Timoshenko theory and needed an additional joint matching technique, but the complexity was compensated by solution accuracy. Because the beam-based analysis of complex structures such as a body-in-white of an automobile plays a critical role in shortening initial design period, the sophistication of the present technique to handle beams of arbitrarily-shaped cross-sections can be an effective analysis tool for initial body design in automotive industry.

Acknowledgments

This research was supported by the National Creative Research Initiatives Program (Korea Science and Technology Foundation grant No. 0420-2008-0011) contracted through the Institute of Advanced Machinery and Design at Seoul National University.

Appendix A

The cross-section shape functions in Eqs. (2) and (3) describing cross-section deformations are given as follows. In the equations below, the subscript i ($i=1,2,3,4$) denotes the edge number of a cross-section and s_i starts from the center of the ith edge. Shape functions not listed below vanish.

Shape functions for in-plane deformations:

$$\psi^{U}_{z_i}=1 \quad (i=1,2,3,4), \tag{A.1}$$

$$\psi^{VI}_{n_1}=-1, \quad \psi^{VI}_{n_3}=1, \quad \psi^{VI}_{s_2}=1, \quad \psi^{VI}_{s_4}=-1, \tag{A.2}$$

$$\psi^{\beta I}_{z_1}=-\frac{b}{2}, \quad \psi^{\beta I}_{z_2}=s, \quad \psi^{\beta I}_{z_3}=\frac{b}{2}, \quad \psi^{\beta I}_{z_4}=-s, \tag{A.3}$$

$$\psi^{WI}_{z_1}(s_1)=-h, \tag{A.4}$$

$$\psi_{z_2}^{WI}(s_2) = \frac{h(b+3h)}{2b} + \frac{3h(b+h)}{b^2}s_2, \tag{A.5}$$

$$\psi_{z_3}^{WI}(s_3) = \frac{3b^2+8bh+3h^2}{2b} - \frac{6(b+3h)(b+h)}{bh^2}s_3^2, \tag{A.6}$$

$$\psi_{z_4}^{WI}(s_4) = \frac{h(b+3h)}{2b} - \frac{3h(b+h)}{b^2}s_4, \tag{A.7}$$

$$\psi_{n_1}^{\chi I}(s_1) = \begin{cases} -\frac{h}{3} + \frac{2}{h}s_1^2 + \frac{4}{3h^2}s_1^3, & \left(-\frac{h}{2} \le s_1 \le 0\right) \\ -\frac{h}{3} + \frac{2}{h}s_1^2 - \frac{4}{3h^2}s_1^3, & \left(0 \le s_1 \le \frac{h}{2}\right) \end{cases}, \tag{A.8}$$

$$\psi_{n_2}^{\chi I}(s_2) = \begin{cases} \frac{b}{3} - \frac{2}{b}s_2^2 - \frac{4}{3b^2}s_2^3, & \left(-\frac{b}{2} \le s_2 \le 0\right) \\ \frac{b}{3} - \frac{2}{b}s_2^2 + \frac{4}{3b^2}s_2^3, & \left(0 \le s_2 \le \frac{b}{2}\right) \end{cases}, \tag{A.9}$$

$$\psi_{n_3}^{\chi I}(s_3) = \psi_{n_1}^{\chi I}(s_1), \quad \psi_{n_4}^{\chi I}(s_4) = \psi_{n_2}^{\chi I}(s_2), \tag{A.10}$$

Shape functions for out-of-plane deformations:

$$\psi_n^{Vo}(s_1) = 0, \quad \psi_n^{Vo}(s_2) = 1, \quad \psi_n^{Vo}(s_3) = 0, \quad \psi_n^{Vo}(s_4) = -1, \tag{A.11}$$

$$\psi_s^{Vo}(s_1) = 1, \quad \psi_s^{Vo}(s_2) = 0, \quad \psi_s^{Vo}(s_3) = -1, \quad \psi_s^{Vo}(s_4) = -1, \tag{A.12}$$

$$\psi_z^{\beta o}(s_1) = s_1, \quad \psi_z^{\beta o}(s_2) = \frac{h}{2}, \quad \psi_z^{\beta o}(s_3) = -s_3, \quad \psi_z^{\beta o}(s_4) = -\frac{h}{2}, \tag{A.13}$$

$$\psi_n^{\theta}(s_i) = -s_i, \quad (i = 1,2,3,4), \tag{A.14}$$

$$\psi_s^{\theta}(s_i) = d \quad (d: \text{ normal distance from the shear center of the cross-section}), \tag{A.15}$$

$$\psi_z^{Wo}(s_1) = \frac{b}{2}s_1, \quad \psi_z^{Wo}(s_2) = -\frac{h}{2}s_2, \quad \psi_z^{Wo}(s_3) = \frac{b}{2}s_3, \quad \psi_z^{Wo}(s_4) = -\frac{h}{2}s_4, \tag{A.16}$$

$$\psi_n^{\chi o}(s_1) = \frac{4}{h(b+h)}s_1^3 - \frac{2b+h}{b+h}s_1, \quad \psi_n^{\chi o}(s_2) = -\frac{4}{b(b+h)}s_2^3 + \frac{b+2h}{b+h}s_2, \tag{A.17}$$

$$\psi_n^{\chi o}(s_3) = \psi_n^{\chi o}(s_1), \quad \psi_n^{\chi o}(s_4) = \psi_n^{\chi o}(s_2), \tag{A.18}$$

$$\psi_s^{\chi o}(s_1)=\frac{bh}{b+h},\quad \psi_s^{\chi o}(s_2)=-\frac{bh}{b+h}, \tag{A.19}$$

$$\psi_s^{\chi o}(s_3)=\frac{bh}{b+h},\quad \psi_s^{\chi o}(s_4)=-\frac{bh}{b+h}. \tag{A.20}$$

The element mass matrix for in-plane deformations (l denotes the length of an element, and r's result from the integration of the products of the cross-section shape functions. The explicit forms of r's will be listed next):

$$\mathbf{M}^I=\rho\begin{bmatrix}
\frac{r_7^I l}{3} & & \frac{r_{10}^I l}{3} & \frac{r_{11}^I l}{3} & & \frac{r_7^I l}{6} & & \frac{r_{10}^I l}{6} & \frac{r_{11}^I l}{6} & \\
& \frac{(r_1^I+r_4^I)l}{3} & & & \frac{(r_3^I+r_6^I)l}{3} & & \frac{(r_1^I+r_4^I)l}{6} & & & \frac{(r_3^I+r_6^I)l}{6} \\
& & \frac{r_8^I l}{3} & \frac{r_{12}^I l}{3} & & \frac{r_{10}^I l}{6} & & \frac{r_8^I l}{6} & \frac{r_{12}^I l}{6} & \\
& & & \frac{r_9^I l}{3} & & \frac{r_{11}^I l}{6} & & \frac{r_{12}^I l}{6} & \frac{r_9^I l}{6} & \\
& & & & \frac{(r_2^I+r_5^I)l}{3} & & \frac{(r_3^I+r_6^I)l}{6} & & & \frac{(r_2^I+r_5^I)l}{6} \\
& & & & & \frac{r_7^I l}{3} & & \frac{r_{10}^I l}{3} & \frac{r_{11}^I l}{3} & \\
& & & & & & \frac{(r_1^I+r_4^I)l}{3} & & & \frac{(r_3^I+r_6^I)l}{3} \\
& & \text{sym} & & & & & \frac{r_8^I l}{3} & \frac{r_{12}^I l}{3} & \\
& & & & & & & & \frac{r_9^I l}{3} & \\
& & & & & & & & & \frac{(r_2^I+r_5^I)l}{3}
\end{bmatrix}. \tag{A.21}$$

The element mass matrix for out-of-plane deformations:

$$\mathbf{M}^O=\rho\begin{bmatrix}
\frac{(r_1^o+r_7^o)l}{3} & & \frac{(r_4^o+r_{11}^o)l}{3} & & \frac{(r_5^o+r_{12}^o)l}{3} & \frac{(r_1^o+r_7^o)l}{6} & & \frac{(r_4^o+r_{11}^o)l}{6} & & \frac{(r_5^o+r_{12}^o)l}{6} \\
& \frac{r_{14}^o l}{3} & & \frac{r_{16}^o l}{3} & & & \frac{r_{14}^o l}{6} & & \frac{r_{16}^o l}{6} & \\
& & \frac{(r_2^o+r_8^o)l}{3} & & \frac{(r_6^o+r_{13}^o)l}{3} & \frac{(r_4^o+r_{11}^o)l}{6} & & \frac{(r_2^o+r_8^o)l}{6} & & \frac{(r_6^o+r_{13}^o)l}{6} \\
& & & \frac{r_{15}^o l}{3} & & & \frac{r_{16}^o l}{6} & & \frac{r_{15}^o l}{6} & \\
& & & & \frac{(r_3^o+r_9^o+r_{10}^o)l}{3} & \frac{(r_5^o+r_{12}^o)l}{6} & & \frac{(r_6^o+r_{13}^o)l}{6} & & \frac{(r_3^o+r_9^o+r_{10}^o)l}{6} \\
& & & & & \frac{(r_1^o+r_7^o)l}{3} & & \frac{(r_4^o+r_{11}^o)l}{3} & & \frac{(r_5^o+r_{12}^o)l}{3} \\
& & & & & & \frac{r_{14}^o l}{3} & & \frac{r_{16}^o l}{3} & \\
& & \text{sym} & & & & & \frac{(r_2^o+r_8^o)l}{3} & & \frac{(r_6^o+r_{13}^o)l}{3} \\
& & & & & & & & \frac{r_{15}^o l}{3} & \\
& & & & & & & & & \frac{(r_3^o+r_9^o+r_{10}^o)l}{3}
\end{bmatrix}. \tag{A.22}$$

The element stiffness matrix for in-plane deformations (s's result from the integration of the products of the cross-section shape functions. The explicit forms of s's will be listed next.):

$$\mathbf{K}^I = \begin{bmatrix}
E_1\frac{s_1^I}{l} & & & E_1\frac{s_4^I}{l} & & E_1\frac{s_6^I}{l} & & & -E_1\frac{s_1^I}{l} & & & -E_1\frac{s_4^I}{l} & & -E_1\frac{s_6^I}{l} & & \\
 & G\frac{s_{10}^I}{l} & & -G\frac{s_{12}^I}{2} & & -G\frac{s_{14}^I}{2} & & & & -G\frac{s_{10}^I}{l} & & -G\frac{s_{12}^I}{2} & & -G\frac{s_{14}^I}{2} & & \\
 & & G\frac{s_8^I l}{3}+E_1\frac{s_2^I}{l} & & G\frac{s_{13}^I l}{3}+E_1\frac{s_5^I}{l} & & & & -E_1\frac{s_4^I}{l} & G\frac{s_{12}^I}{2} & & G\frac{s_8^I l}{6}-E_1\frac{s_2^I}{l} & & G\frac{s_{13}^I l}{6}-E_1\frac{s_5^I}{l} & & \\
 & & & G\frac{s_9^I l}{3}+E_1\frac{s_3^I}{l} & & & & & -E_1\frac{s_6^I}{l} & G\frac{s_{14}^I}{2} & & G\frac{s_{13}^I l}{6}-E_1\frac{s_5^I}{l} & & G\frac{s_9^I l}{6}-E_1\frac{s_3^I}{l} & & \\
 & & & & E_1\frac{s_7^I l}{3}+G\frac{s_{11}^I}{l} & & & & & & & & & & E_1\frac{s_7^I l}{6}-G\frac{s_{11}^I}{l} \\
 & & & & & & E_1\frac{s_1^I}{l} & & & E_1\frac{s_4^I}{l} & & E_1\frac{s_6^I}{l} & & & \\
 & & & & & & & G\frac{s_{10}^I}{l} & & G\frac{s_{12}^I}{2} & & G\frac{s_{14}^I}{2} & & & \\
 & & & \text{sym} & & & & & G\frac{s_8^I l}{3}+E_1\frac{s_2^I}{l} & & G\frac{s_{13}^I l}{3}+E_1\frac{s_5^I}{l} & & & & \\
 & & & & & & & & & G\frac{s_9^I l}{3}+E_1\frac{s_3^I}{l} & & & & & \\
 & & & & & & & & & & & & & E_1\frac{s_7^I l}{3}+G\frac{s_{11}^I}{l} &
\end{bmatrix}. \tag{A.23}$$

The element stiffness matrix for out-of-plane deformations:

$$\mathbf{K}^O = \begin{bmatrix}
G\frac{s_4^o}{l} & & -G\frac{s_9^o}{2} & & & & -G\frac{s_4^o}{l} & & -G\frac{s_9^o}{2} & & & & & & \\
 & G\frac{s_5^o l}{3}+E_1\frac{s_1^o}{l} & & & & & G\frac{s_9^o}{2} & & G\frac{s_5^o l}{6}-E_1\frac{s_1^o}{l} & & & & & & \\
 & & & G\frac{s_7^o}{l} & & -G\frac{s_{10}^o}{2} & & G\frac{s_{12}^o}{l} & & & & -G\frac{s_7^o}{l} & & -G\frac{s_{10}^o}{2} & & -G\frac{s_{12}^o}{l} \\
 & & & & G\frac{s_6^o l}{3}+E_1\frac{s_2^o}{l} & & -G\frac{s_{11}^o}{2} & & & & & G\frac{s_{10}^o}{2} & & G\frac{s_6^o l}{6}-E_1\frac{s_2^o}{l} & & G\frac{s_{11}^o}{2} \\
 & & & & & E_1\frac{s_3^o l}{3}+G\frac{s_8^o}{l} & & & & & & -G\frac{s_{12}^o}{l} & & -G\frac{s_{11}^o}{2} & & E_1\frac{s_3^o l}{6}-G\frac{s_8^o}{l} \\
 & & & & & & G\frac{s_4^o}{l} & & G\frac{s_9^o}{2} & & & & & & \\
 & & & & & & & G\frac{s_5^o l}{3}+E_1\frac{s_1^o}{l} & & & & & & & \\
 & & & \text{sym} & & & & & & & & G\frac{s_7^o}{l} & & G\frac{s_{10}^o}{2} & & G\frac{s_{12}^o}{l} \\
 & & & & & & & & & & & & G\frac{s_6^o l}{3}+E_1\frac{s_2^o}{l} & & G\frac{s_{11}^o}{2} & \\
 & & & & & & & & & & & & & & E_1\frac{s_3^o l}{3}+G\frac{s_8^o}{l}
\end{bmatrix}. \tag{A.24}$$

$$r_1^I = \int (\psi_n^{VI})^2\,\mathrm{d}A = 2ht, \quad r_2^I = \int (\psi_n^{\chi I})^2\,\mathrm{d}A = \frac{34t(h^3+b^3)}{315}, \quad r_3^I = \int \psi_n^{\chi I}\psi_n^{VI}\,\mathrm{d}A = 0, \tag{A.25}$$

$$r_4^I = \int (\psi_s^{VI})^2\,\mathrm{d}A = 2bt, \quad r_5^I = \int \left(n\frac{\mathrm{d}\psi_n^{\chi I}}{\mathrm{d}s}\right)^2\mathrm{d}A = \frac{4t^3(h+b)}{45}, \quad r_6^I = -\int n\frac{\mathrm{d}\psi_n^{\chi I}}{\mathrm{d}s}\psi_s^{VI}\,\mathrm{d}A = 0, \tag{A.26}$$

$$r_7^I = \int (\psi_z^U)^2 \, dA = 2t(h+b), \quad r_8^I = \int (\psi_z^{\beta I})^2 \, dA = t\left(\frac{hb^2}{2} + \frac{b^3}{6}\right), \tag{A.27}$$

$$r_9^I = \int (\psi_z^{WI})^2 \, dA = \frac{ht(9h^4 + 54h^3 b + 77h^2 b^2 + 38hb^3 + 6b^4)}{5b^2}, \tag{A.28}$$

$$r_{10}^I = \int \psi_z^U \psi_z^{\beta I} \, dA = 0, \quad r_{11}^I = \int \psi_z^U \psi_z^{WI} \, dA = 0, \quad r_{12}^I = \int \psi_z^{\beta I} \psi_z^{WI} \, dA = 0, \tag{A.29}$$

$$r_1^o = \int (\psi_n^{Vo})^2 \, dA = 2bt, \quad r_2^o = \int (\psi_n^{\theta})^2 \, dA = \frac{t(h^3 + b^3)}{6}, \tag{A.30}$$

$$r_3^o = \int (\psi_n^{\chi o})^2 \, dA = \frac{2t(2h^4 + 12h^3 b + 23h^2 b^2 + 12hb^3 + 2b^4)}{105(h+b)}, \tag{A.31}$$

$$r_4^o = \int \psi_n^{Vo} \psi_n^{\theta} \, dA = 0, \quad r_5^o = \int \psi_n^{Vo} \psi_n^{\chi o} \, dA = 0, \quad r_6^o = \int \psi_n^{\theta} \psi_n^{\chi o} \, dA = \frac{t(h^3 + 4h^2 b - 4hb^2 - b^3)}{15}, \tag{A.32}$$

$$r_7^o = \int (\psi_s^{Vo})^2 \, dA = 2ht, \quad r_8^o = \int (\psi_s^{\theta})^2 \, dA = \frac{hbt(h+b)}{2}, \quad r_9^o = \int (\psi_s^{\chi o})^2 \, dA = \frac{2h^2 b^2 t}{h+b}, \tag{A.33}$$

$$r_{10}^o = \int \left(n \frac{d\psi_n^{\chi o}}{ds}\right)^2 dA = \frac{2t^3(h^2 + 4hb + b^2)}{15(h+b)}, \quad r_{11}^o = \int \psi_s^{Vo} \psi_s^{\theta} \, dA = 0, \quad r_{12}^o = \int \psi_s^{Vo} \psi_s^{\chi o} \, dA = 0, \tag{A.34}$$

$$r_{13}^o = \int \psi_s^{\theta} \psi_s^{\chi o} \, dA = 0, \quad r_{14}^o = \int (\psi_z^{\beta})^2 \, dA = t\left(\frac{h^3}{6} + \frac{h^2 b}{2}\right), \quad r_{15}^o = \int (\psi_z^{Wo})^2 \, dA = \frac{h^2 b^2 t(h+b)}{24}, \tag{A.35}$$

$$r_{16}^o = \int \psi_z^{\beta o} \psi_z^{Wo} \, dA = 0, \tag{A.36}$$

$$s_1^I = \int_A (\psi_z^U)^2 \, dA = 2t(b+h), \quad s_2^I = \int_A (\psi_z^{\beta I})^2 \, dA = t\left(\frac{b^2 h}{2} + \frac{b^3}{6}\right), \tag{A.37}$$

$$s_3^I = \int_A (\psi_z^{WI})^2 \, dA = \frac{ht(6b^4 + 38b^3 h + 77b^2 h^2 + 54bh^3 + 9h^4)}{5b^2}, \quad s_4^I = \int_A \psi_z^U \psi_z^{\beta I} \, dA = 0, \tag{A.38}$$

$$s_5^I = \int_A \psi_z^{\beta I} \psi_z^{WI} \, dA = 0, \quad s_6^I = \int_A \psi_z^{WI} \psi_z^U \, dA = 0, \quad s_7^I = \int_A \left(n \frac{d^2 \psi_n^{\chi I}}{ds^2}\right)^2 dA = \frac{t^3(8b + 8h)}{9}, \tag{A.39}$$

$$s_8^I = \int_A \left(\frac{\mathrm{d}\psi_z^{\beta I}}{\mathrm{d}s}\right)^2 \mathrm{d}A = 2bt, \quad s_9^I = \int_A \left(\frac{\mathrm{d}\psi_z^{WI}}{\mathrm{d}s}\right)^2 \mathrm{d}A = \frac{6t(b+h)^2(2b^3+12b^2h+18bh^2+3h^3)}{b^3h}, \tag{A.40}$$

$$s_{10}^I = \int_A (\psi_s^{VI})^2 \,\mathrm{d}A = 2bt, \quad s_{11}^I = \int_A \left(n\frac{\mathrm{d}\psi_n^{\chi I}}{\mathrm{d}s}\right)^2 \mathrm{d}A = \frac{28t^3(b+h)}{315}, \quad s_{12}^I = \int_A \frac{\mathrm{d}\psi_z^{\beta I}}{\mathrm{d}s}\psi_s^{VI}\,\mathrm{d}A = 2bt, \tag{A.41}$$

$$s_{13}^I = \int_A \frac{\mathrm{d}\psi_z^{\beta I}}{\mathrm{d}s}\frac{\mathrm{d}\psi_z^{WI}}{\mathrm{d}s}\,\mathrm{d}A = \frac{6ht(b+h)}{b}, \quad s_{14}^I = \int_A \psi_s^{VI}\frac{\mathrm{d}\psi_z^{WI}}{\mathrm{d}s}\,\mathrm{d}A = \frac{6ht(b+h)}{b}, \tag{A.42}$$

$$s_1^o = \int_A (\psi_z^{\beta o})^2 \,\mathrm{d}A = \frac{h^2t(h+3b)}{6}, \quad s_2^o = \int_A (\psi_z^{Wo})^2 \,\mathrm{d}A = \frac{b^2h^2t(b+h)}{24}, \tag{A.43}$$

$$s_3^o = \int_A n^2\left(\frac{\mathrm{d}^2\psi_n^{\chi o}}{\mathrm{d}s^2}\right)^2 \mathrm{d}A = \frac{8t^3}{b+h}, \quad s_4^o = \int_A (\psi_s^{Vo})^2 \,\mathrm{d}A = 2ht, \quad s_5^o = \int_A \left(\frac{\mathrm{d}\psi_z^{\beta o}}{\mathrm{d}s}\right)^2 \mathrm{d}A = 2ht, \tag{A.44}$$

$$s_6^o = \int_A \left(\frac{\mathrm{d}\psi_z^{Wo}}{\mathrm{d}s}\right)^2 \mathrm{d}A = \frac{hbt(h+b)}{2}, \quad s_7^o = \int_A (\psi_s^{\theta})^2 \,\mathrm{d}A = \frac{hbt(h+b)}{2}, \tag{A.45}$$

$$s_8^o = \int_A \left[(\psi_s^{\chi o})^2 + \left(n\frac{\mathrm{d}\psi_n^{\chi o}}{\mathrm{d}s}\right)^2\right]\mathrm{d}A = \frac{2b^2h^2t}{b+h} + \frac{2t^3(b^2+4bh+h^2)}{15(b+h)}, \quad s_9^o = \int_A \frac{\mathrm{d}\psi_z^{\beta o}}{\mathrm{d}s}\psi_s^V\,\mathrm{d}A = 2ht, \tag{A.46}$$

$$s_{10}^o = \int_A \frac{\mathrm{d}\psi_z^{Wo}}{\mathrm{d}s}\psi_s^{\theta}\,\mathrm{d}A = \frac{hbt(b-h)}{2}, \quad s_{11}^o = \int_A \frac{\mathrm{d}\psi_z^{Wo}}{\mathrm{d}s}\psi_s^{\chi o}\,\mathrm{d}A = \frac{-2b^2h^2t}{b+h}, \quad s_{12}^o = \int_A \psi_s^{\theta}\psi_s^{\chi o}\,\mathrm{d}A = 0. \tag{A.47}$$

The three-dimensional displacements on Joint Section J:

On Edge 2

$${}^2\tilde{u}_{A_J,n_J}^I(n_J,s_J) = \psi_n^{\chi I}\chi_A^I, \tag{A.48}$$

$${}^2\tilde{u}_{A_J,s_J}^I(n_J,s_J) = U_A\sin\phi + V_A^I\cos\phi - n_J\frac{\mathrm{d}\psi_n^{\chi I}}{\mathrm{d}s}\chi_A^I\cos\phi + \psi_z^{WI}W_A^I\sin\phi, \tag{A.49}$$

$${}^2\tilde{u}_{A_J,z_J}^I(n_J,s_J) = U_A\cos\phi - V_A^I\sin\phi + s_J\beta_A^I + n_J\frac{\mathrm{d}\psi_n^{\chi I}}{\mathrm{d}s}\chi_A^I\sin\phi + \psi_z^{WI}W_A^I\cos\phi, \tag{A.50}$$

$${}^2\tilde{u}_{A_J,n_J}^o(n_J,s_J) = V_A^o - s_J\theta_A\cos\phi - s_J\beta_A^o\sin\phi + \psi_n^{\chi o}\chi_A^o, \tag{A.51}$$

$${}^2\tilde{u}_{A_J,s_J}^o(n_J,s_J) = \frac{h}{2}\theta_A\cos\phi + \frac{h}{2}\beta_A^o\sin\phi - \frac{h}{2}s_JW_A^o\sin\phi - \frac{bh}{b+h}\chi_A^o\cos\phi - n_J\frac{\mathrm{d}\psi_n^{\chi o}}{\mathrm{d}s}\chi_A^o, \tag{A.52}$$

$${}^2\tilde{u}_{A_J,z_J}^o(n_J,s_J) = \frac{h}{2}\beta_A^o\cos\phi - \frac{h}{2}\theta_A\sin\phi - \frac{h}{2}s_JW_A^o\cos\phi + \frac{bh}{b+h}\chi_A^o\sin\phi. \tag{A.53}$$

On Edge 3

$${}^3\tilde{u}_{A_J,n_J}^I(n_J,s_J) = U_A\sin\phi + V_A^I\cos\phi + \psi_n^{\chi I}\chi_A^I\cos\phi + \psi_z^{WI}W_A^I\sin\phi, \tag{A.54}$$

$$ {}^{3}\tilde{u}^{I}_{A_J,s_J}(n_J,s_J) = -n_J \frac{\mathrm{d}\psi^{\chi I}_n}{\mathrm{d}s}\chi^I_A, \tag{A.55} $$

$$ {}^{3}\tilde{u}^{I}_{A_J,z_J}(n_J,s_J) = U_A\cos\phi - V^I_A\sin\phi + \frac{b}{2}\beta^I_A - \psi^{\chi I}_n\chi^I_A\sin\phi + \psi^{WI}_z W^I_A\cos\phi, \tag{A.56} $$

$$ {}^{3}\tilde{u}^{o}_{A_J,n_J}(n_J,s_J) = -s_J\beta^o_A\sin\phi - s_J\theta_A\cos\phi - \frac{b}{2}s_J W^o_A\sin\phi + \psi^{\chi o}_n\chi^o_A\cos\phi, \tag{A.57} $$

$$ {}^{3}\tilde{u}^{o}_{A_J,s_J}(n_J,s_J) = -V^o_A + \frac{b}{2}\beta^o_A\sin\phi + \frac{b}{2}\theta_A\cos\phi + \frac{bh}{b+h}\chi^o_A - n_J\frac{\mathrm{d}\psi^{\chi o}_n}{\mathrm{d}s}\chi^o_A, \tag{A.58} $$

$$ {}^{3}\tilde{u}^{o}_{A_J,z_J}(n_J,s_J) = s_J\beta^o_A\cos\phi - s_J\theta_A\sin\phi + \frac{b}{2}s_J W^o_A\cos\phi + \psi^{\chi o}_n\chi^o_A\sin\phi. \tag{A.59} $$

On Edge 4

$$ {}^{4}\tilde{u}^{I}_{A_J,n_J}(n_J,s_J) = \psi^{\chi I}_n\chi^I_A, \tag{A.60} $$

$$ {}^{4}\tilde{u}^{I}_{A_J,s_J}(n_J,s_J) = -U_A\sin\phi - V^I_A\cos\phi - n_J\frac{\mathrm{d}\psi^{\chi I}_n}{\mathrm{d}s}\chi^I_A\cos\phi - \psi^{WI}_z W^I_A\sin\phi, \tag{A.61} $$

$$ {}^{4}\tilde{u}^{I}_{A_J,z_J}(n_J,s_J) = U_A\cos\phi - V^I_A\sin\phi - s_J\beta^I_A - n_J\frac{\mathrm{d}\psi^{\chi I}_n}{\mathrm{d}s}\chi^I_A\sin\phi + \psi^{WI}_z W^I_A\cos\phi \tag{A.62} $$

$$ {}^{4}\tilde{u}^{o}_{A_J,n_J}(n_J,s_J) = -V^o_A - s_J\theta_A\cos\phi - s_J\beta^o_A\sin\phi + \psi^{\chi o}_n\chi^o_A, \tag{A.63} $$

$$ {}^{4}\tilde{u}^{o}_{A_J,s_J}(n_J,s_J) = \frac{h}{2}\theta_A\cos\phi + \frac{h}{2}\beta^o_A\sin\phi - \frac{h}{2}s_J W^o_A\sin\phi - \frac{bh}{b+h}\chi^o_A\cos\phi - n_J\frac{\mathrm{d}\psi^{\chi o}_n}{\mathrm{d}s}\chi^o_A. \tag{A.64} $$

$$ {}^{4}\tilde{u}^{o}_{A_J,z_J}(n_J,s_J) = \frac{h}{2}\beta^o_A\cos\phi - \frac{h}{2}\theta_A\sin\phi - \frac{h}{2}s_J W^o_A\cos\phi + \frac{bh}{b+h}\chi^o_A\sin\phi \tag{A.65} $$

References

[1] G. Prater, A.M. Shahhosseini, E.Y. Kuo, P.R. Mehta, V.T. Furman, Finite element concept model for vehicle architecture assessment and optimization, Society of Automotive Engineers Paper 2005-01-1400, 2005.
[2] E.Y. Kuo, G. Prater, A.M. Shahhosseini, P.R. Mehta, Reliability and quality of body concept CAE models for design direction studies, Society of Automotive Engineers Paper 2006-01-1617, 2006.
[3] T. Nakagawa, H. Nishigaki, Y. Tsurumi, N. Kikuchi, First order analysis for automotive body structure design—part 4: noise and vibration analysis applied to a subframe, Society of Automotive Engineers Paper 2004-01-1661, 2004.
[4] H. Nishigaki, S. Nishiwaki, T. Amago, Y. Kojima, N. Kikuchi, First order analysis—new CAE tools for automotive body designers, Society of Automotive Engineers Paper 2001-01-0768, 2001.
[5] Y.M. Moon, T.H. Jee, Y.P. Park, Development of an automotive joint model using an analytically based formulation, *Journal of Sound and Vibration* 220 (4) (1999) 625–640.
[6] K. Lee, E. Nikolaidis, A two-dimensional model for joints in vehicle structures, *Computers & Structures* 45 (4) (1992) 775–784.
[7] M.E.M. El-Sayed, Calculation of joint spring rates using finite element formulation, *Computers & Structures* 33 (4) (1989) 977–981.
[8] Y.Y. Kim, H.J. Lim, J.H. Kang, J.H. Kim, Reconsideration of the joint modeling technique: in a box-beam T-joint, *Proceedings of the Ninth International Conference on Vehicle Structural Mechanics and CAE*, Paper No. 951094, Troy, MI, USA, April 4–6, 1995, pp. 275–279.
[9] J.H. Kim, Y.Y. Kim, Analysis of thin-walled closed beams with general quadrilateral cross sections, *ASME Journal of Applied Mechanics* 66 (1999) 904–912.
[10] J.H. Kim, Y.Y. Kim, One-dimensional analysis of thin-walled closed beam having general cross sections, *International Journal for Numerical Methods in Engineering* 49 (2000) 653–668.
[11] J.H. Kim, H.S. Kim, D.W. Kim, Y.Y. Kim, New accurate efficient modeling techniques for the vibration analysis of T-joint thin-walled box structures, *International Journal of Solids and Structures* 39 (2002) 2893–2909.
[12] G.W. Jang, K.J. Kim, Y.Y. Kim, Higher-order beam analysis of box beams connected at angled joints subject to out-of-plane bending and torsion, *International Journal for Numerical Methods in Engineering* 75 (11) (2008) 1361–1384.
[13] G.W. Jang, Y.Y. Kim, Higher-order in-plane bending analysis of box beams connected at an angled joint considering cross-sectional bending warping and distortion, 2008, submitted.
[14] G.R. Liu, S.S. Quek, *The Finite Element Method: A Practical Course*, Butterworth-Heinemann, Oxford, 2003.
[15] The Mathworks Inc., Matlab User's Guide for Symbolic Math Toolbox, Release 14, 2004.
[16] ANSYS Inc., ANSYS Structural Analysis Guide, 2007.
[17] Y.Y. Kim, Y. Kim, A one-dimensional theory of thin-walled curved rectangular box beams under torsion and out-of-plane bending, *International Journal for Numerical Methods in Engineering* 53 (2002) 1675–1693.
[18] Y. Kim, Y.Y. Kim, Analysis of thin-walled curved box beam under in-plane flexure, *International Journal of Solids and Structures* 40 (2003) 6111–6123.